Optimal Energy Conserving and Energy Dissipative Local Discontinuous Galerkin Methods for the Benjamin–Bona–Mahony Equation

Xiaole Li[1,2] · **Yulong Xing**[2] · **Ching-Shan Chou**[2]

Abstract

We develop, analyze and numerically validate local discontinuous Galerkin (LDG) methods for solving the nonlinear Benjamin–Bona–Mahony (BBM) equation. With appropriately chosen numerical fluxes, the conventional LDG methods can be shown to preserve the discrete version of mass, and either preserve or dissipate the discrete version of energy, up to the round-off level. The error estimate with optimal order of convergence is provided for both the semi-discrete energy conserving and energy dissipative methods applied to the nonlinear BBM equation, by a novel technique to discover the connection between the error of the auxiliary and primary variables, and by carefully analyzing the nonlinear term. Fully discrete methods can be derived with energy-conserving implicit midpoint temporal discretization. Numerical experiments confirm the optimal rates of convergence, as well as the mass and energy conserving/dissipative property. The comparison of the long time behavior of the energy conserving and energy dissipative methods are also provided, to show that the energy conserving method produces a better approximation to the exact solution. In a recent study by Fu and Shu (J Comput Phys 394:329–363, 2019), optimal energy conserving discontinuous Galerkin methods based on doubling-the-unknowns technique were developed for the linear symmetric hyperbolic systems. We extend the idea to construct another class of energy conserving LDG methods for the nonlinear BBM equation. Their energy conservation property and optimal convergence rate (via a special constructed numerical projection) are investigated. We also provide a comparison of these two types of energy conserving LDG methods, and shown that, under the same setup of computational elements, the latter method produces a smaller numerical error with slightly longer computational time.

Extended author information available on the last page of the article

1 Introduction

The dynamics of shallow water wave equations can be modeled by the nonlinear dispersive wave equation, for example, the nonlinear Korteweg–de Vries (KdV) equation

$$u_t + u_x + u_{xxx} + uu_x = 0,$$

which has been used in a wide range of applications [1]. In 1972, Benjamin et al. [2] proposed an improved version of the KdV equation that also models long shallow water waves of small amplitude, known as the Benjamin–Bona–Mahony (BBM) equation

$$u_t + u_x - u_{xxt} + uu_x = 0.$$

The BBM equation is obtained by replacing the third-order term u_{xxx} in the KdV equation with a mixed derivative term u_{xxt}, and demonstrates some attractive features that the KdV equation lacks, one specific example being better dispersion properties resulting in improved stability of the high wavenumber components. The BBM equation describes the unidirectional propagation of surface water in a nonlinear dispersive medium with small amplitude and long wave [2], and has been used in the analysis of hydromagnetic waves in cold plasma, acoustic-gravity waves in compressible fluids and acoustic waves in harmonic crystals [3]. Due to its wide applications and rich dynamics, researchers have developed many different forms of BBM equations which are usually called generalized BBM equations, see [4,5] and the references therein.

In this paper, we consider the BBM equation taking the form of

$$u_t - \varepsilon u_{xxt} + uu_x = 0, \tag{1.1}$$

on the interval $I = [x_l, x_r]$, with the periodic boundary condition

$$u(x_l, t) = u(x_r, t), \tag{1.2}$$

and the initial condition

$$u(x, 0) = u_0(x), \tag{1.3}$$

where $\varepsilon > 0$ is a given real number. The BBM equation possesses the *cnoidal-wave* solutions of the form

$$u(x, t; C, D, m) = \frac{3mC}{(2m-1)} cn^2 \left(\frac{1}{2\sqrt{(2m-1)\varepsilon}}(x - Ct - D); m \right) \tag{1.4}$$

where $cn(z; m)$ is the Jacobi elliptic function with modulus $m \in (0, 1)$ (see [6]). $C > 0$ is the speed of propagation of the solitary wave, and D is an arbitrary, real translation. The period of *cnoidal-wave* solutions is $2K(m)/B$, where $K(m)$ is the complete elliptic integral of the first kind and $B = \frac{1}{2\sqrt{(2m-1)\varepsilon}}$. It is well known that the BBM equation possesses two invariant quantities: the mass $M(t)$ and energy $E(t)$, defined by

$$M(t) := \int_I u(x, t) dx, \tag{1.5}$$

and

$$E(t) := \int_I \left(u^2(x, t) + \varepsilon u_x^2(x, t) \right) dx. \tag{1.6}$$

There have been a wide range of theoretical work available for the BBM equation. Here we briefly review a few of them. The global existence, uniqueness and stability of the solutions of

one-dimensional BBM equation were studied in [2]. The result was extended in [7,8] to multi-dimensional cases. The existence and uniqueness of the periodic solutions was discussed in [9], and that of the solitary wave solutions was studied in [10]. Numerical solutions of the BBM equation have been studied by many researchers. We refer to [5,11,12] for the studies of the convergence analysis of various finite difference and finite element methods proposed for the BBM equation. High order scheme based on the local discontinuous Galerkin (LDG) finite element method has been presented in [13,14] for one class of Sobolev equations which includes the BBM equation. Numerical stability, as well as the optimal error estimate when upwind nonlinear numerical flux was used, were studied in these papers. Another set of LDG method was proposed in [15] for the KdV–BBM equation. In [16], LDG methods with two different sets of numerical fluxes to either preserve or dissipate energy was proposed for the Boussinesq coupled BBM system, and optimal error estimate was provided for the linearized equations.

We confine our discussion on the high order discontinuous Galerkin (DG) method [17–21] in this paper. It is a class of finite element methods using completely discontinuous piecewise polynomial basis functions, and inherits the benefits of both finite element and finite volume methods. Advantages of DG methods are many, including the flexibility for hp-adaptivity, efficient parallel implementation, the local conservativity, the ability for easy handling of complicated geometries and boundary conditions, and easy coordination with finite volume techniques, making the methods very attractive in a wide range of applications. The LDG methods were proposed by Cockburn and Shu in [22] to numerically solve partial differential equations (PDEs) containing high order spatial derivatives terms, and we refer to the review paper [23] for the development of LDG methods. Recently, there have been many studies in designing DG and LDG methods which can conserve the energy or Hamiltonian structure of the model in the discrete level. Energy conserving LDG methods have been designed for the generalized KdV equation [24–27], the second order wave equation [28,29], the two-way wave equation [30], the Camassa–Holm equation [31], the Degasperis-Procesi equation [32], the nonlinear Schrödinger equation [33,34] and the improved Boussinesq equation [35].

In this paper, we develop, analyze and numerically validate two classes of LDG methods for solving the nonlinear BBM equation. By introducing one auxiliary variable, and with appropriately chosen numerical fluxes, the conventional LDG methods can be shown to preserve the discrete version of mass, and either preserve or dissipate the discrete version of energy of the continuous solution, up to the round-off level, which leads to the numerical stability automatically. The proposed LDG method takes a different formulation from that in [13], where three auxiliary variables were introduced for discretize the high order derivative term. Our method is closer to the one in [15], but with a wide choice of numerical fluxes to derive both energy conserving and dissipative methods. One main contribution of this paper is to provide an optimal a priori error estimate for both the semi-discrete energy conserving and energy dissipative methods applied to the nonlinear BBM equation. In [13, 15], optimal error estimate has been obtained for the upwind nonlinear numerical fluxes only, and the same analysis cannot be extended to the energy conserving methods presented here. Few work has been done in the literature on providing optimal error estimate for the energy conserving methods applied to nonlinear equations. To achieve this goal, we discover the connection between the error of the auxiliary and primary variables, and use this connection to bound the nonlinear term by the auxiliary variable. Fully discrete methods can be derived by coupling with energy-conserving implicit midpoint temporal discretization. Numerical experiments confirm the optimal rates of convergence, as well as the mass and energy conserving/dissipative property. The comparison of the long time behavior of the energy conserving and energy dissipative methods are also provided, to show that the energy

conserving method produces a better approximation to the exact solution, especially for long time simulation and when polynomial degree k is small.

Recently, based on the idea of doubling the unknown functions via introducing auxiliary zero functions, optimal energy conserving DG methods have been presented for linear symmetric hyperbolic systems by Fu and Shu in [36]. The same idea has been extended in [37] to provide an energy conserving ultra-weak DG method for the KdV equation, where comparison with existing energy conserving or dissipative DG methods have been provided to demonstrate the better performance of the new developed optimal energy conserving DG methods. At the end of the paper, another class of energy conserving LDG methods, based on this doubling-the-unknowns technique in [36], is also constructed for the nonlinear BBM equation. We investigate their energy conservation property and optimal convergence rate via a special constructed numerical projection. We also provide a comparison of these two types of energy conserving LDG methods presented in this paper, and under the same setup of computational elements, the latter method is shown to have a smaller numerical error with only slightly longer computational time.

Another motivation of the study of the energy conserving methods for the BBM equation originates from our recent work in [31], where the energy conserving LDG method for the Camassa–Holm equation was investigated. In [31, Figure 2], the comparison of numerical solutions by the energy conserving and dissipative methods with the exact solution is provided, where we can observe a smaller phase error of the energy conserving methods, but the improvement in terms of the phase error is not as good as that for the KdV [24] and Degasperis-Procesi [32] equations. This phenomenon was also mentioned in [31]. We expect this study of energy conserving methods for the simpler BBM equation provides us some insights on this matter, and we will discuss our observation in the numerical experiment section.

The organization of the paper is as follows. In Sect. 2, we present the LDG method for the nonlinear BBM equation, and show that energy conserving or dissipative methods can be obtained by choosing appropriate parameters and fluxes. The optimal error estimate of the proposed methods is provided. Energy conserving temporal discretization is presented to obtain fully discrete methods, which are shown to preserve the discrete version of mass, and either preserve or dissipate the discrete version of energy of the continuous solution, up to the round-off level. Numerical results are provided in Sect. 3 to show the order of accuracy, the mass and energy conservation property and long time behavior of the LDG numerical solutions. In Sect. 4, we introduce another class of energy conserving LDG methods based on doubling-the-unknowns technique, recently proposed in [36]. Energy conserving property and optimal error estimate of these methods have been studied. In Sect. 5, numerical tests are provided to show the performance of the second class of energy conserving method, as well as the numerical comparison of these two classes of LDG methods. Conclusion remarks are presented in Sect. 6.

2 The LDG Method

In this section, we start by applying the conventional LDG method to the BBM equation, and show that the energy conserving/dissipative methods can be achieved with suitable choices of numerical fluxes. The proof of optimal error estimate for the proposed energy conserving/dissipative LDG method applied to the nonlinear BBM equation is also provided, and we end the section by presenting the temporal discretization which is also energy conserving.

2.1 Notations

We divide the computational domain $I = [x_l, x_r]$ into J subintervals and denote the cells by $I_j = [x_{j-\frac{1}{2}}, x_{j+\frac{1}{2}}]$ for $j = 1, 2, \ldots, J$. The center of each cell is $x_j = \frac{1}{2}(x_{j+\frac{1}{2}} + x_{j-\frac{1}{2}})$, and the mesh size is denoted by $h_j = x_{j+\frac{1}{2}} - x_{j-\frac{1}{2}}$ with $h = \max h_j$ for $j = 1, 2, \ldots, J$ being the maximal mesh size. We assume that the mesh is regular, namely, the ratio between the maximal and the minimal mesh sizes stays bounded during mesh refinement. The piecewise polynomial space V_h^k is defined as the space of polynomials of degree up to k in each cell I_j, that is,

$$V_h^k = \{v : v|_{I_j} \in P^k(I_j), \ j = 1, 2, \ldots, J\}.$$

The solution of the numerical scheme is denoted by u_h, which belongs to the finite element space V_h^k. We denote by $(u_h)_{j+\frac{1}{2}}^+$ and $(u_h)_{j+\frac{1}{2}}^-$ the limit values of u_h at $x_{j+\frac{1}{2}}$ from the right cell I_{j+1} and from the left cell I_j, respectively. We use the usual notations

$$[u_h] = u_h^+ - u_h^-, \quad \{u_h\} = \frac{1}{2}(u_h^+ + u_h^-)$$

to respectively represent the jump and the mean of the function u_h at the element interfaces, for which we have the following equalities summarized in the lemma.

Lemma 2.1 *Assuming $u_h, v_h \in V_h^k$, we have the equalities*

$$[u_h v_h]_{j+\frac{1}{2}} = \begin{cases} \left(u_h^+[v_h] + [u_h]v_h^-\right)_{j+\frac{1}{2}}, \\ \left(u_h^-[v_h] + [u_h]v_h^+\right)_{j+\frac{1}{2}}, \\ \left(\{u_h\}[v_h] + [u_h]\{v_h\}\right)_{j+\frac{1}{2}}. \end{cases}$$

If u is continuous at the point $x_{j+\frac{1}{2}}$, we have $\{u\}_{j+\frac{1}{2}} = u_{j+\frac{1}{2}}$, $[u]_{j+\frac{1}{2}} = 0$, and the above equality reduces to

$$[u v_h]_{j+\frac{1}{2}} = (u[v_h])_{j+\frac{1}{2}}.$$

For a shorthand notation, the inner product is denoted by $(w, v)_j = \int_{I_j} wv\,dx$ for the scalar variables w, v. Finally, we provide the definition of various norms that will be used in the rest of the paper.

- $\|v\|$: the L^2 norm of a function $v \in L^2(I)$;
- $\|v\|_\infty$: the L^∞ norm of a function $v \in L^2(I)$;
- $\|v\|_{\Gamma_h} = \sqrt{\sum_{j=1}^J \left(v^2(x_{j+\frac{1}{2}}^+) + v^2(x_{j+\frac{1}{2}}^-)\right)}$: the norm defined on the element interfaces;
- $|[v]| = \sqrt{\sum_{j=1}^J [v]_{j-\frac{1}{2}}^2}$: the so called "jump semi-norm".

2.2 The Semi-discrete LDG Method

To derive the LDG discretization of the BBM Eq. (1.1), we introduce the auxiliary variable $v = u_x$ and rewrite the equation as

$$\begin{cases} u_t - \varepsilon v_{xt} + f(u)_x = 0, \\ v = u_x, \end{cases} \tag{2.1}$$

where $f(u) = u^2/2$ is the flux term. The LDG spatial discretization of the system (2.1) is given as follows: we seek u_h and $v_h \colon [0, T] \to V_h^k$, the numerical approximations of u and v, such that the variation forms

$$(u_{h,t}, \phi_1)_j + \varepsilon \mathcal{H}_j^*(v_{h,t}, \phi_1; \widehat{v_{h,t}}) - \mathcal{F}_j^*(u_h, \phi_1; \widehat{f}) = 0, \tag{2.2a}$$

$$(v_h, \phi_2)_j + \mathcal{H}_j^*(u_h, \phi_2; \widehat{u_h}) = 0, \tag{2.2b}$$

hold in each cell I_j, $j = 1, 2, \ldots, J$, for any test function $\phi_1, \phi_2 \in V_h^k$. The bilinear forms in the Eq. (2.2) are defined as

$$\mathcal{H}_j^*(\varphi, \psi; \widehat{\varphi}) = (\varphi, \psi_x)_j - (\widehat{\varphi}\psi^-)_{j+\frac{1}{2}} + (\widehat{\varphi}\psi^+)_{j-\frac{1}{2}}, \tag{2.3}$$

$$\mathcal{F}_j^*(\varphi, \psi; \widehat{f}) = (f(\varphi), \psi_x)_j - (\widehat{f}\psi^-)_{j+\frac{1}{2}} + (\widehat{f}\psi^+)_{j-\frac{1}{2}}, \tag{2.4}$$

where the hatted terms, $\widehat{u_h}$, $\widehat{f}$ and $\widehat{v_{h,t}}$ in the Eq. (2.2), are the so-called numerical fluxes, defined on the numerical solutions values at the element interfaces. We will specify how to choose these numerical fluxes later. For the bilinear forms $\mathcal{H}_j^*$, we have following observations:

Lemma 2.2 *Assuming $\varphi, \psi \in V_h^k$ are both periodic functions, the following equalities hold*

$$\sum_{j=1}^{J} \mathcal{H}_j^*(\varphi, \psi; \widehat{\varphi})_j = \sum_{j=1}^{J} (\varphi, \psi_x)_j + \sum_{j=1}^{J} (\widehat{\varphi}[\psi])_{j-\frac{1}{2}}, \tag{2.5}$$

and

$$\sum_{j=1}^{J} \left(\mathcal{H}_j^*(\varphi, \psi; \widehat{\varphi})_j + \mathcal{H}_j^*(\psi, \varphi; \widehat{\psi})_j \right) = \begin{cases} \displaystyle\sum_{j=1}^{J} \left((\widehat{\varphi} - \varphi^+)[\psi] + (\widehat{\psi} - \psi^-)[\varphi] \right)_{j-\frac{1}{2}}, \\[1.2em] \displaystyle\sum_{j=1}^{J} \left((\widehat{\varphi} - \varphi^-)[\psi] + (\widehat{\psi} - \psi^+)[\varphi] \right)_{j-\frac{1}{2}}, \\[1.2em] \displaystyle\sum_{j=1}^{J} \left((\widehat{\varphi} - \{\varphi\})[\psi] + (\widehat{\psi} - \{\psi\})[\varphi] \right)_{j-\frac{1}{2}}. \end{cases} \tag{2.6}$$

Proof The Eq. (2.5) follows directly from the definition (2.3) and the periodicity of φ, ψ. From the integration by parts and the periodicity, we have

$$\sum_{j=1}^{J} (\varphi, \psi_x)_j = -\sum_{j=1}^{J} (\varphi_x, \psi)_j - \sum_{j=1}^{J} [\varphi\psi]_{j-\frac{1}{2}}. \tag{2.7}$$

Therefore, the Eq. (2.6) can be obtained from the combination of the Eqs. (2.5), (2.7) and Lemma 2.1. □

The next theorem shows that the LDG methods (2.2) ensure the conservation of the total mass.

Theorem 2.1 *Let u_h, v_h be the solutions of scheme (2.2) with any choice of consistent numerical fluxes, and define the discrete mass as*

$$M_h(t) = \sum_{j=1}^{J} \int_{I_j} u_h dx,$$

then we have

$$M_h(t) = M_h(0).$$

Proof By taking the test function $\phi_1 = 1$ in the first equation of (2.2) and summing up over all cells, we have

$$\sum_{j=1}^{J} (u_{h,t}, 1)_j + \varepsilon \sum_{j=1}^{J} \mathcal{H}_j^*(v_{h,t}, 1; \widehat{v_{h,t}}) - \sum_{j=1}^{J} \mathcal{F}_j^*(u_h, 1; \widehat{f}) = 0.$$

It is easy to see that

$$\sum_{j=1}^{J} (u_{h,t}, 1)_j = \frac{1}{2} \frac{d}{dt} M_h(t),$$

$$\sum_{j=1}^{J} \mathcal{H}_j^*(v_{h,t}, 1; \widehat{v_{h,t}}) = \sum_{j=1}^{J} (v_{h,t}, 0)_j + \sum_{j=1}^{J} (\widehat{v}_{h,t}[1])_{j-\frac{1}{2}} = 0,$$

$$\sum_{j=1}^{J} \mathcal{F}_j^*(u_h, 1; \widehat{f}) = \sum_{j=1}^{J} (f(u_h), 0)_j + \sum_{j=1}^{J} (\widehat{f}[1])_{j-\frac{1}{2}} = 0.$$

Therefore we obtain

$$\frac{d}{dt} M_h(t) = 0.$$

which leads to $M_h(t) = M_h(0)$.   □

In order to find numerical fluxes that conserve or dissipate the total energy $E(t)$ at the semi-discrete level, we start with the following result:

Lemma 2.3 *Let u_h, v_h be the numerical solutions of the LDG methods (2.2), the following energy equation holds*

$$\frac{1}{2} \frac{d}{dt} \sum_{j=1}^{J} \int_{I_j} \left(u_h^2 + \varepsilon v_h^2 \right) dx + \sum_{j=1}^{J} \left([F(u_h)] - \widehat{f}[u_h] \right)_{j-\frac{1}{2}}$$

$$+ \varepsilon \sum_{j=1}^{J} \left((\widehat{v_{h,t}} - v_{h,t}^*)[u_h] + (\widehat{u_h} - u_h^*)[v_{h,t}] \right)_{j-\frac{1}{2}} = 0, \tag{2.8}$$

where $F(u) = \int^u f(s)ds$ and the pair $\langle u_h^*, v_{h,t}^* \rangle_{j-\frac{1}{2}}$ can be any choice from the sets $\langle u_h^+, v_{h,t}^- \rangle_{j-\frac{1}{2}}$, $\langle u_h^-, v_{h,t}^+ \rangle_{j-\frac{1}{2}}$ and $\langle \{u_h\}, \{v_{h,t}\} \rangle_{j-\frac{1}{2}}$ for any j.

Proof By taking $\phi_1 = u_h$ and $\phi_2 = \varepsilon v_{h,t}$ in (2.2), adding those two equations and then summing up over all cells, we have

$$\sum_{j=1}^{J} \left((u_{h,t}, u_h)_j + \varepsilon(v_h, v_{h,t})_j \right) - \sum_{j=1}^{J} \mathcal{F}_j^*(u_h, u_h; \widehat{f})$$

$$+ \varepsilon \sum_{j=1}^{J} \left(\mathcal{H}_j^*(v_{h,t}, u_h; \widehat{v_{h,t}}) + \mathcal{H}_j^*(u_h, v_{h,t}; \widehat{u_h}) \right) = 0.$$

The first two terms can be rewritten as

$$\sum_{j=1}^{J} \left((u_{h,t}, u_h)_j + \varepsilon(v_h, v_{h,t})_j \right) = \frac{1}{2} \frac{d}{dt} \sum_{j=1}^{J} \int_{I_j} \left(u_h^2 + \varepsilon v_h^2 \right) dx.$$

By applying Lemma 2.2, we can obtain

$$\sum_{j=1}^{J} \left(\mathcal{H}_j^*(v_{h,t}, u_h; \widehat{v_{h,t}}) + \mathcal{H}_j^*(u_h, v_{h,t}; \widehat{u_h}) \right)$$

$$= \sum_{j=1}^{J} \int_{I_j} \left((\widehat{v_{h,t}} - v_{h,t}^*)[u_h] + (\widehat{u_h} - u_h^*)[v_{h,t}] \right)_{j+\frac{1}{2}},$$

with the choice of the pair $\langle u_h^*, v_{h,t}^* \rangle_{j-\frac{1}{2}}$ stated in the theorem, and

$$\sum_{j=1}^{J} \mathcal{F}_j^*(u_h, u_h; \widehat{f}(u_h)) = \sum_{j=1}^{J} (f(u_h), u_{h,x})_j + \sum_{j=1}^{J} (\widehat{f}[u_h])_{j-\frac{1}{2}}$$

$$= \sum_{j=1}^{J} F(u_h)\big|_{\partial I_j} + \sum_{j=1}^{J} (\widehat{f}[u_h])_{j-\frac{1}{2}} = -\sum_{j=1}^{J} \left([F(u_h)] - \widehat{f}[u_h] \right)_{j+\frac{1}{2}}.$$

The combination of all these equations above leads to the energy Eq. (2.8). □

Motivated by this lemma, the following choices of numerical fluxes have been investigated in this paper. For the pair of the numerical fluxes $(\widehat{u_h}, \widehat{v_{h,t}})$, we choose them to be

$$\begin{cases} \widehat{v_{h,t}} = v_{h,t}^* + c_u[u_h], \\ \widehat{u_h} = u_h^*, \end{cases} \tag{2.9}$$

where $c_u \geq 0$ and $(u_h^*, v_{h,t}^*)$ can be either $(\cdot^+, \cdot^-)$ or $(\cdot^-, \cdot^+)$. Recently, there have been some studies on upwind-biased fluxes for approximating the first order derivative term [38], and generalized alternating numerical fluxes [39] for approximating the diffusion term. The term $(u_h^*, v_{h,t}^*)$ can also be extended to the generalized alternating numerical fluxes in the form of

$$\left(\{u_h\} - \alpha[u_h], \{v_{h,t}\} + \alpha[v_{h,t}] \right), \tag{2.10}$$

which won't affect the energy conserving/dissipative property of the resulting methods. For the nonlinear advection term $f(u) = \frac{1}{2}u^2$, we can choose either the conservative flux

$$\widehat{f}(u^-, u^+) = \frac{1}{u^+ - u^-} \int_{u^-}^{u^+} f(s)ds = \frac{1}{6} \left((u^+)^2 + (u^-)^2 + u^+u^- \right), \tag{2.11}$$

or the standard local Lax-Friedrichs flux

$$\widehat{f}(u^-, u^+) = \frac{(u^+)^2 + (u^-)^2}{4} - \frac{\max(|u^+|, |u^-|)}{2}[u]. \tag{2.12}$$

It is easy to observe that the conservative flux (2.11) satisfies

$$\widehat{f}(u, u) = f(u) = \frac{1}{2}u^2, \quad \sum_{j=1}^{J} \left([F(u_h)] - \widehat{f}(u_h)[u_h]\right)_{j+\frac{1}{2}} = 0,$$

where $F(u) = u^3/6$. The Lax-Friedrichs flux (2.12) is a nondecreasing function of its first argument, and a nonincreasing function of its second argument, and satisfies

$$\widehat{f}(u, u) = f(u) = \frac{1}{2}u^2, \quad \sum_{j=1}^{J} \left([F(u_h)] - \widehat{f}(u_h)[u_h]\right)_{j+\frac{1}{2}} \geq 0.$$

With these choices of numerical fluxes, the following observation on energy conservation or energy dissipation holds, as a result of Lemma 2.3.

Theorem 2.2 *Let u_h, v_h be the numerical solutions of LDG scheme* (2.2), *with the numerical fluxes $(\widehat{u_h}, \widehat{v_{h,t}})$ chosen as* (2.9) *with $c_u = 0$, and the numerical flux of the nonlinear term $\widehat{f}$ chosen as* (2.11). *The following energy conservation property holds*

$$E_h(t) \doteq \int_I \left(u_h^2(x, t) + \varepsilon v_h^2(x, t)\right) dx = E_h(0).$$

Theorem 2.3 *Let u_h, v_h be the numerical solutions of LDG scheme* (2.2), *with the numerical fluxes $(\widehat{u_h}, \widehat{v_{h,t}})$ chosen as* (2.9) *with $c_u \geq 0$, and the numerical flux of the nonlinear term $\widehat{f}$ chosen as either* (2.11) *or* (2.12). *The following energy dissipative property holds*

$$E_h(t_1) \leq E_h(t_2) \leq E_h(0), \quad \forall\, t_1 \geq t_2 \geq 0. \tag{2.13}$$

Remark 2.1 Another popular choice of energy conserving numerical fluxes is the central flux, that can be define as

$$\widehat{v_h} = \{v_h\}, \quad \widehat{u_h} = \{u_h\}, \quad \widehat{f}(u^-, u^+) \text{ chosen as (2.11)}.$$

The LDG scheme (2.2) combined with this set of numerical fluxes exhibit suboptimal convergence rate, which will be observed in the accuracy numerical tests.

Remark 2.2 In [13], LDG methods are derived for the BBM Eq. (1.1) based on an equivalent formulation

$$\begin{cases} u_t = w, \\ w + (f(u) - \varepsilon p)_x = 0, \\ p - w_x = 0, \end{cases} \tag{2.14}$$

with two auxiliary variables w and p. Its difference to our approach lies in the discretization of the term u_{xxt} which is linear. Therefore, if the numerical fluxes $(\widehat{u_h}, \widehat{v_{h,t}})$ take the same form as $(\widehat{w_h}, \widehat{p_h})$ [in the discretization of (2.14)], and the same nonlinear numerical flux $\widehat{f}$ is used, these two LDG methods can be shown to be equivalent, after all these auxiliary variables are eliminated and only one final equation to update u_h is obtained. Energy dissipative methods have been discussed in [13]. More choices of numerical fluxes, leading to energy conserving or dissipative methods, are discussed in this paper, as well as the optimal error estimate for these fluxes which requires some new analytical tools to be discussed in the following section.

2.3 Optimal Error Estimate

In this section, we derive the optimal error estimate for the LDG scheme (2.2), with the numerical fluxes $(\widehat{u_h}, \widehat{v_{h,t}})$ chosen as (2.9) with $c_u \geq 0$, and the numerical flux of the nonlinear term $\widehat{f}(u^-, u^+)$ chosen as either (2.11) or (2.12). In other words, optimal error estimate will be provided for both energy conserving and energy dissipative LDG methods.

We start by defining the following errors associated with a function f

$$e_f = f - f_h = \eta_f - \xi_f, \qquad \eta_f = f - \pi^f f, \qquad \xi_f = f_h - \pi^f f,$$

which from left to right, denote the error between the exact solution f and the numerical solution f_h, the projection error between f and a particular projection π^f of f, and the error between the numerical solution and the projection of f, respectively.

Some projection operators considered in this paper are defined as follows. We use π to denote the standard L^2 projection of a function ω into the space V_h^k, satisfying

$$(\pi\omega, \phi)_j = (\omega, \phi)_j, \quad \forall \phi \in P^k(I_j).$$

We use π^- to denote the Radau projection of ω into the space V_h^k, satisfying

$$(\pi^-\omega, \phi)_j = (\omega, \phi)_j, \quad \forall \phi \in P^{k-1}(I_j),$$
$$(\pi^-\omega)^- = \omega^-, \quad \text{at } x_{j+\frac{1}{2}}.$$

Similarly, the projection π^+ of ω is defined as:

$$(\pi^+\omega, \phi)_j = (\omega, \phi)_j, \quad \forall \phi \in P^{k-1}(I_j),$$
$$(\pi^+\omega)^+ = \omega^+, \quad \text{at } x_{j-\frac{1}{2}}.$$

For these three projections, we have the following approximation property [28,40]:

$$\|\pi^f f - f\|^2 + h\|\pi^f f - f\|_{\Gamma_h}^2 + h^2\|\pi^f f - f\|_\infty^2 \leq Ch^{2k+2}, \tag{2.15}$$

where $\pi^f = \pi, \pi^\pm$ and the constant C depends on f but is independent of h. For our problem, we choose the projections of the solutions u and v to be:

$$\pi^v = \pi, \qquad \pi^u = \begin{cases} \pi^+, & \text{if } \widehat{u_h} = u_h^+, \\ \pi^-, & \text{if } \widehat{u_h} = u_h^-. \end{cases} \tag{2.16}$$

Moreover, for all $v \in V_h^k$ the following inverse inequalities holds

$$\|v_x\| \leq Ch^{-1}\|v\|, \tag{2.17}$$
$$\|v\|_{\Gamma_h} \leq Ch^{-1/2}\|v\|, \tag{2.18}$$
$$\|v\|_\infty \leq Ch^{-1/2}\|v\|. \tag{2.19}$$

Before we present the main result on the optimal error estimate of the LDG scheme, let us start by providing some useful lemmas.

Lemma 2.4 *Suppose $(u_h, v_h) \in V_h^k \times V_h^k$ satisfy the Eq. (2.2b) with the flux $\widehat{u_h} = u_h^-$ or $\widehat{u_h} = u_h^+$, and the projections (2.16) are used, then there exists a positive constant C independent of h such that*

$$\|\xi_{u,x}\| + h^{-1/2}|[\xi_u]| \leq C\|\xi_v\|. \tag{2.20}$$

Remark 2.3 This Lemma provides an important relationship between the error of the auxiliary variable and the primary variable. In [41, Lemma 2.4], similar result on the variable instead of the error

$$\|u_{h,x}\| + h^{-1/2}|[u_h]| \leq C\|v_h\|,$$

has been obtained, and the main body of our proof follows that in [41].

Proof Without loss of generality, we assume $\widehat{u_h} = u_h^+$, and the proof of the other case $\widehat{u_h} = u_h^-$ follows the same idea. From (2.2b) and (2.3), we have

$$-(v_h, \phi)_j = \mathcal{H}_j^*(u_h, \phi; \widehat{u_h}) = (u_h, \phi_x)_j - (\widehat{u_h}\phi^-)_{j+\frac{1}{2}} + (\widehat{u_h}\phi^+)_{j-\frac{1}{2}},$$

and the same equation is satisfied by the exact solutions u and v. Taking the difference yields the error equation

$$
\begin{aligned}
-(e_v, \phi)_j = -(\xi_v + \eta_v, \phi)_j &= (e_u, \phi_x)_j - (\widehat{e_u}\phi^-)_{j+\frac{1}{2}} + (\widehat{e_u}\phi^+)_{j-\frac{1}{2}} \\
&= (\xi_u + \eta_u, \phi_x)_j - ((\widehat{\xi_u} + \widehat{\eta_u})\phi^-)_{j+\frac{1}{2}} + ((\widehat{\xi_u} + \widehat{\eta_u})\phi^+)_{j-\frac{1}{2}}.
\end{aligned}
$$

By utilizing the definition of the projections π and $\pi^{\pm}$, we have

$$
\begin{aligned}
-(\xi_v, \phi)_j &= (\xi_u, \phi_x)_j - (\widehat{\xi_u}\phi^-)_{j+\frac{1}{2}} + (\widehat{\xi_u}\phi^+)_{j-\frac{1}{2}} \\
&= -(\xi_{u,x}, \phi)_j + (\xi_u^- - \widehat{\xi_u})\phi^-|_{j+\frac{1}{2}} - (\xi_u^+ - \widehat{\xi_u})\phi^+|_{j-\frac{1}{2}} \qquad (2.21) \\
&= -(\xi_{u,x}, \phi)_j - [\xi_u]\phi^-|_{j+\frac{1}{2}},
\end{aligned}
$$

where the integration by parts and $\widehat{\xi_u} = \xi_u^+$ are used.

The rest of the proof follows that of [41, Lemma 2.4], and we only sketch the main idea below. Let L_k be the standard Legendre polynomial of degree k in $[-1, 1]$, we have $L_k(1) = 1$ and L_k is orthogonal to any polynomials with degree less or equal to $k - 1$. First, we take the test function ϕ as

$$\phi(x)\big|_{I_j} = \xi_{u,x}(x) - \xi_{u,x}(x_{j+\frac{1}{2}}^-)L_k(\theta),$$

with $\theta = 2(x - x_j)/h_j$. Therefore, the Eq. (2.21) reduces to

$$
\begin{aligned}
\|\xi_{u,x}\|_{I_j}^2 \doteq (\xi_{u,x}, \xi_{u,x})_j &= -(\xi_{u,x}, \phi)_j - [\xi_u]\phi^-|_{j+\frac{1}{2}} \\
&= -(\xi_v, \phi)_j \leq \|\xi_v\|_{I_j}\|\phi\|_{I_j} \leq C\|\xi_v\|_{I_j}\|\xi_{u,x}\|_{I_j},
\end{aligned}
$$

which leads to

$$\|\xi_{u,x}\|_{I_j} \leq C\|\xi_v\|_{I_j}. \qquad (2.22)$$

Next, we take $\phi = 1$ in (2.21) to obtain

$$h^{-\frac{1}{2}}[\xi_u]_{j+\frac{1}{2}} = h^{-\frac{1}{2}}\left((\xi_v, 1)_j - (\xi_{u,x}, 1)_j\right) \leq h^{-\frac{1}{2}}\|1\|_{I_j}(\|\xi_v\|_{I_j} + \|\xi_{u,x}\|_{I_j}) \leq C\|\xi_v\|_{I_j},$$

$$(2.23)$$

by the Cauchy–Schwarz inequality and (2.22). Finally, by summing up (2.22) and (2.23) over all elements, we get the desired result (2.20). $\qquad \square$

Remark 2.4 To deal with the nonlinear term, we would like to make an a priori error estimate assumption between numerical solution u_h and exact solution u

$$\|u - u_h\| \leq h,$$

following the setup in [40,42], where the same technique is used to treat the nonlinearity in the KdV and Keller–Segel models. This assumption can be easily verified, and we refer to [40,42] for the detailed explanation and proof. Easy to observe that this assumption implies

$$\|u - u_h\|_\infty \leq \|u - \pi u\|_\infty + \|\pi u - u_h\|_\infty \leq C, \tag{2.24}$$

following the inverse inequality (2.19).

Lemma 2.5 *Let u_h, v_h be the numerical solutions of the LDG scheme* (2.2) *with the numerical fluxes $(\widehat{u_h}, \widehat{v_{h,t}})$ chosen as* (2.9) *with $c_u \geq 0$, and the numerical flux of the nonlinear term $\widehat{f}(u^-, u^+)$ chosen as either* (2.11) *or* (2.12). *Assume that u is the exact solution of the problem* (1.1) *and is sufficiently smooth, then there holds the following inequality*

$$\left| \sum_{j=1}^{J} \mathcal{F}_j^*(u_h, \xi_u; \widehat{f}(u_h^-, u_h^+)) - \sum_{j=1}^{J} \mathcal{F}_j^*(u, \xi_u; f(u)) \right|$$
$$\leq C \|\xi_u\|^2 + C \left(\|\partial_x \xi_u\|^2 + h^{-1} |[\xi_u]|^2 \right) + Ch^{2k+2}. \tag{2.25}$$

Proof We start by showing that both u and u_h are bounded. The exact solution u satisfies the energy invariant property (1.6), hence, we have

$$E(t) = \|u(x,t)\|^2 + \varepsilon \|u_x(x,t)\|^2 = E(0).$$

By Trace inequality, one can obtain that $\|u(x,t)\|_\infty < C$ for any t, where C depends only on the initial condition $u_0(x)$ and the domain I. Combining this with (2.24) leads to $\|u_h\|_\infty < C$ as well.

To prove the estimate (2.25), we separate the left hand side into two terms as follows:

$$\sum_{j=1}^{J} \left| \mathcal{F}_j^*(u_h, \xi_u; \widehat{f}(u_h^-, u_h^+)) - \mathcal{F}_j^*(u, \xi_u; f(u)) \right|$$
$$= \sum_{j=1}^{J} \left| (f(u_h) - f(u), \partial_x \xi_u)_j + \left(\widehat{f}(u_h^-, u_h^+) - f(u) \right)_{j-\frac{1}{2}} [\xi_u]_{j-\frac{1}{2}} \right| := \sum_{j=1}^{J} \left| \theta_j^1 + \theta_j^2 \right|. \tag{2.26}$$

Since $f(u) = \frac{1}{2}u^2$, it follows from the Cauchy-Schwarz inequality, the inverse inequality and projection error bound (2.15) that

$$\sum_{j=1}^{J} |\theta_j^1| = \sum_{j=1}^{J} \left| \left(\frac{1}{2}(u_h + u)(u_h - u), \partial_x \xi_u \right)_j \right| \leq C \|u_h - u\| \|\partial_x \xi_u\|$$
$$= C \|\xi_u - \eta_u\| \|\partial_x \xi_u\| \leq C \|\xi_u\|^2 + C \|\partial_x \xi_u\|^2 + Ch^{2k+2}. \tag{2.27}$$

The estimation of the second term θ_j^2 will be treated differently, depending on the different choices of the numerical fluxes $\widehat{f}(u_h^-, u_h^+)$. If the conservative flux (2.11) is used, by applying the mean-value theorem, we can get

$$
\sum_{j=1}^{J} |\theta_j^2| = \sum_{j=1}^{J} \left| (\widehat{f}(u_h^-, u_h^+) - f(u))_{j-\frac{1}{2}} [\xi_u]_{j-\frac{1}{2}} \right| = \sum_{j=1}^{J} \left| (\widehat{f}(u_h^-, u_h^+) - \widehat{f}(u, u))_{j-\frac{1}{2}} [\xi_u]_{j-\frac{1}{2}} \right|
$$

$$
\leq \sum_{j=1}^{J} \left(\left| \frac{\partial \widehat{f}}{\partial u^-}(\sigma_{1,j}, \sigma_{2,j}) \right| |u_h^- - u| + \left| \frac{\partial \widehat{f}}{\partial u^+}(\sigma_{1,j}, \sigma_{2,j}) \right| |u_h^+ - u| \right)_{j-\frac{1}{2}} \left| [\xi_u]_{j-\frac{1}{2}} \right|
$$

$$
= \frac{1}{6} \sum_{j=1}^{J} \left(|2\sigma_{1,j} + \sigma_{2,j}| |u_h^- - u| + |\sigma_{1,j} + 2\sigma_{2,j}| |u_h^+ - u| \right)_{j-\frac{1}{2}} \left| [\xi_u]_{j-\frac{1}{2}} \right|
$$

$$
\leq C \sum_{j=1}^{J} \left(|u_h^- - u| + |u_h^+ - u| \right)_{j-\frac{1}{2}} \left| [\xi_u]_{j-\frac{1}{2}} \right|, \tag{2.28}
$$

where $\sigma_{1,j} = (\alpha_{1,j} u_h^- + (1 - \alpha_{1,j})u)_{j-\frac{1}{2}}$ and $\sigma_{2,j} = (\alpha_{2,j} u_h^+ + (1 - \alpha_{2,j})u)_{j-\frac{1}{2}}$ for some $\alpha_{1,j}, \alpha_{2,j} \in [0, 1]$, and the last inequality follows from

$$
\left| \frac{\partial \widehat{f}}{\partial u^-}(\sigma_{1,j}, \sigma_{2,j}) \right| = \frac{1}{6} |2\sigma_{1,j} + \sigma_{2,j}| \leq C, \qquad \left| \frac{\partial \widehat{f}}{\partial u^+}(\sigma_{1,j}, \sigma_{2,j}) \right| = \frac{1}{6} |\sigma_{1,j} + 2\sigma_{2,j}| \leq C,
$$

since $\|u\|_\infty < C$ and $\|u_h\|_\infty < C$. When $\widehat{f}(u_h^-, u_h^+)$ is chosen as the Lax-Friedrichs flux (2.12), we have

$$
\sum_{j=1}^{J} |\theta_j^2| = \sum_{j=1}^{J} \left| (\widehat{f}(u_h^-, u_h^+) - f(u))_{j-\frac{1}{2}} [\xi_u]_{j-\frac{1}{2}} \right|
$$

$$
= \sum_{j=1}^{J} \left| \left(\frac{1}{4} ((u_h^+)^2 + (u_h^-)^2 + 2\max(|u_h^+|, |u_h^-|)(u_h^+ - u_h^-)) - \frac{1}{2} u^2 \right)_{j-\frac{1}{2}} [\xi_u]_{j-\frac{1}{2}} \right|
$$

$$
\leq \frac{1}{4} \sum_{j=1}^{J} \left| \left((u_h^+ + u)(u_h^+ - u) + (u_h^- + u)(u_h^- - u) \right)_{j-\frac{1}{2}} [\xi_u]_{j-\frac{1}{2}} \right|
$$

$$
+ \frac{1}{2} \sum_{j=1}^{J} \left| \left(\max(|u_h^+|, |u_h^-|)((u_h^+ - u) - (u_h^- - u)) \right)_{j-\frac{1}{2}} [\xi_u]_{j-\frac{1}{2}} \right|
$$

$$
\leq C \sum_{j=1}^{J} \left(|u_h^- - u| + |u_h^+ - u| \right)_{j-\frac{1}{2}} \left| [\xi_u]_{j-\frac{1}{2}} \right|. \tag{2.29}
$$

Therefore, it follows from (2.28) and (2.29) that, for either choice of the nonlinear flux $\widehat{f}(u_h^-, u_h^+)$,

$$
\sum_{j=1}^{J} |\theta_j^2| \leq C \sum_{j=1}^{J} \left(|u_h^- - u| + |u_h^+ - u| \right)_{j-\frac{1}{2}} \left| [\xi_u]_{j-\frac{1}{2}} \right|
$$

$$
\leq C \sum_{j=1}^{J} h^{\frac{1}{2}} \left(|\xi_u^- - \eta_u^-| + |\xi_u^+ - \eta_u^+| \right)_{j-\frac{1}{2}} \left(h^{-\frac{1}{2}} |[\xi_u]_{j-\frac{1}{2}}| \right)
$$

$$\leq C \left(h\|\eta_u\|_{\Gamma_h}^2 + h\|\xi_u\|_{\Gamma_h}^2 + h^{-1}|[\xi_u]|^2 \right)$$

$$\leq C \left(\|\xi_u\|^2 + h^{-1}|[\xi_u]|^2 + h^{2k+2} \right). \tag{2.30}$$

The combination of the Eqs. (2.26), (2.27) and (2.30) leads to the desired result (2.25), and this finishes the proof.   □

Remark 2.5 The above lemma to bound the error in approximating the nonlinear term is one of the key ideas to derive the optimal error estimate. In this paper, we consider the nonlinear BBM equation with $f(u) = \frac{1}{2}u^2$. For the general flux $f(u)$, the lemma also holds, if the numerical flux $\widehat{f}(u^-, u^+)$ is a monotone numerical flux consistent with f. Therefore, the optimal error estimate result in Theorem 2.4 holds for the LDG methods applied to the general equation of the form $u_t + f(u)_x - \epsilon u_{xxt} = 0$.

Remark 2.6 The initial condition of the LDG scheme (2.2) is chosen as

$$u_h(x, 0) = \pi^u u_0(x) \tag{2.31}$$

and $v_h(x, 0)$ is calculated by (2.2b). With the choice of π^u defined in (2.16), one can follow the proof in [28] to show the following estimate:

$$\|\xi_u(0)\| = 0, \quad \|\xi_v(0)\| \leq Ch^{k+1}. \tag{2.32}$$

Now, we can present and prove the main optimal error estimate result for both energy conserving and energy dissipative LDG methods.

Theorem 2.4 *Let u_h and v_h be the numerical solutions of LDG scheme (2.2) with the numerical fluxes $(\widehat{u_h}, \widehat{v_{h,t}})$ chosen as (2.9) with $c_u \geq 0$, and the numerical flux of the nonlinear term $\widehat{f}(u^-, u^+)$ chosen as either (2.11) or (2.12). Assuming u is the exact solution of the problem (1.1) which is sufficiently smooth, and $v = u_x$. For small h and all $t \in [0, T]$, the optimal error estimate*

$$\|e_u\| \leq Ch^{k+1}, \quad \|e_v\| \leq Ch^{k+1}, \tag{2.33}$$

holds, where the constant C may depend on T, k, the length of the domain I, and some Sobolev norms of the exact solution u up to time T, but is independent of h.

Proof The numerical solutions u_h, v_h satisfy the LDG scheme (2.2)–(2.2b), which are also satisfied by the exact solutions u and v. The difference of these equations yields the error equations

$$(\xi_{u_t}, \phi_1)_j + \varepsilon \mathcal{H}_j^*(\xi_{v_t}, \phi_1; \widehat{\xi_{v_t}}) - \mathcal{F}_j^*(u_h, \phi_1; \widehat{f}(u_h^-, u_h^+))$$
$$= (\eta_{u_t}, \phi_1)_j + \varepsilon \mathcal{H}_j^*(\eta_{v_t}, \phi_1; \widehat{\eta_{v_t}}) - \mathcal{F}_j^*(u, \phi_1; f(u)), \tag{2.34}$$

$$(\xi_v, \phi_2)_j + \mathcal{H}_j^*(\xi_u, \phi_2; \widehat{\xi_u}) = (\eta_v, \phi_2)_j + \mathcal{H}_j^*(\eta_u, \phi_2; \widehat{\eta_u}). \tag{2.35}$$

By taking the test functions $\phi_1 = \xi_u$ in (2.34), $\phi_2 = \varepsilon \xi_{v_t}$ in (2.35), and summing those equations, we have

$$\sum_{j=1}^{J} \left((\xi_{u_t}, \xi_u)_j + \varepsilon(\xi_v, \xi_{v_t})_j \right) + \varepsilon \sum_{j=1}^{J} \left(\mathcal{H}_j^*(\xi_{v_t}, \xi_u; \widehat{\xi_{v_t}}) + \mathcal{H}_j^*(\xi_u, \xi_{v_t}; \widehat{\xi_u}) \right)$$

$$= \sum_{j=1}^{J} \left((\eta_{u_t}, \xi_u)_j + \varepsilon(\eta_v, \xi_{v_t})_j \right) + \sum_{j=1}^{J} \left(\mathcal{F}_j^*(u_h, \xi_u; \widehat{f}(u_h^-, u_h^+)) - \mathcal{F}_j^*(u, \xi_u; f(u)) \right)$$

$$+ \varepsilon \sum_{j=1}^{J} \left(\mathcal{H}_j^*(\eta_{v_t}, \xi_u; \widehat{\eta_{v_t}}) + \mathcal{H}_j^*(\eta_u, \xi_{v_t}; \widehat{\eta_u}) \right). \tag{2.36}$$

Following the property of the operator $\mathcal{H}_j$ in (2.6) and the selection of numerical flux in (2.9), we can obtain

$$\varepsilon \sum_{j=1}^{J} \left(\mathcal{H}_j^*(\xi_{v_t}, \xi_u; \widehat{\xi_{v_t}}) + \mathcal{H}_j^*(\xi_u, \xi_{v_t}; \widehat{\xi_u}) \right) = \varepsilon \sum_{j=1}^{J} c_u [\xi_u]_{j-\frac{1}{2}}^2.$$

The other property (2.5) of the operator $\mathcal{H}_j$ leads to

$$\varepsilon \sum_{j=1}^{J} \left(\mathcal{H}_j^*(\eta_{v_t}, \xi_u; \widehat{\eta_{v_t}}) + \mathcal{H}_j^*(\eta_u, \xi_{v_t}; \widehat{\eta_u}) \right)$$

$$= \varepsilon \sum_{j=1}^{J} \left((\eta_{v_t}, \partial_x \xi_u)_j + (\eta_u, \partial_x \xi_{v_t})_j \right) + \varepsilon \sum_{j=1}^{J} \left(\widehat{\eta_{v_t}}[\xi_u] + \widehat{\eta_u}[\xi_{v_t}] \right)_{j-\frac{1}{2}}.$$

Therefore, the Eq. (2.36) can be rewritten as

$$\frac{1}{2} \frac{d}{dt} \left(\|\xi_u\|^2 + \varepsilon \|\xi_v\|^2 \right) = -\varepsilon c_u [[\xi_u]]^2 + \sum_{j=1}^{J} (\eta_{u_t}, \xi_u)_j + \varepsilon \sum_{j=1}^{J} (\eta_v, \xi_{v_t})_j$$

$$+ \sum_{j=1}^{J} \left(\mathcal{F}_j^*(u_h, \xi_u; \widehat{f}(u_h^-, u_h^+)) - \mathcal{F}_j^*(u, \xi_u; f(u)) \right) \tag{2.37}$$

$$+ \varepsilon \sum_{j=1}^{J} \left((\eta_{v_t}, \partial_x \xi_u)_j + (\eta_u, \partial_x \xi_{v_t})_j \right) + \varepsilon \sum_{j=1}^{J} \left(\widehat{\eta_{v_t}}[\xi_u] + \widehat{\eta_u}[\xi_{v_t}] \right)_{j-\frac{1}{2}}.$$

From the choice (2.16) of our projections of u and v, it follows that

$$\varepsilon \sum_{j=1}^{J} (\eta_v, \xi_{v_t})_j = 0, \quad \sum_{j=1}^{J} \widehat{\eta_u}[\xi_{v_t}]_{j-\frac{1}{2}} = 0, \tag{2.38}$$

and

$$\varepsilon \sum_{j=1}^{J} \left((\eta_{v_t}, \partial_x \xi_u)_j + (\eta_u, \partial_x \xi_{v_t})_j \right) = 0. \tag{2.39}$$

By the properties (2.15) of projection error and Young's inequality, we have

$$\sum_{j=1}^{J} (\eta_{u_t}, \xi_u)_j \leq \|\eta_{u_t}\|^2 + \|\xi_u\|^2 \leq Ch^{2k+2} + \|\xi_u\|^2. \tag{2.40}$$

The combination of the inequality (2.25) in Lemma 2.5 and the inequality (2.20) in Lemma 2.4 yields

$$\left| \sum_{j=1}^{J} \mathcal{F}_j^*(u_h, \xi_u; \widehat{f}(u_h^-, u_h^+)) - \sum_{j=1}^{J} \mathcal{F}_j^*(u, \xi_u; f(u)) \right| \leq C \left(\|\xi_u\|^2 + \|\xi_v\|^2 \right) + Ch^{2k+2}.$$

(2.41)

The definition of $\widehat{\eta_{v_t}}$ in (2.9) leads to

$$\begin{aligned}
\varepsilon \sum_{j=1}^{J} \left(\widehat{\eta_{v_t}}[\xi_u] \right)_{j-\frac{1}{2}} &= \varepsilon \sum_{j=1}^{J} \left((\eta_{v_t}^* + c_u[\eta_u])[\xi_u] \right)_{j-\frac{1}{2}} \\
&\leq \frac{\varepsilon}{2} \sum_{j=1}^{J} \left(h(\eta_{v_t}^*)^2 + h[\eta_u]^2 + (c_u^2 + 1)h^{-1}[\xi_u]^2 \right)_{j-\frac{1}{2}} \quad (2.42) \\
&\leq \frac{\varepsilon}{2} h \|\eta_{v_t}\|_{\Gamma_h}^2 + \frac{\varepsilon}{2} h \|\eta_u\|_{\Gamma_h}^2 + \frac{\varepsilon(c_u^2 + 1)}{2} h^{-1} |[\xi_u]|^2 \\
&\leq Ch^{2k+2} + C\|\xi_v\|^2,
\end{aligned}$$

where the assumption $c_u \geq 0$ is used, and the last inequality follows from the projection error bound (2.15) and Lemma 2.4. By combining (2.38)–(2.42), one can rewrite Eq. (2.37) as

$$\frac{d}{dt} \left(\|\xi_u\|^2 + \varepsilon \|\xi_v\|^2 \right) \leq C \left(\|\xi_u\|^2 + \varepsilon \|\xi_v\|^2 \right) + Ch^{2k+2}.$$

The optimal error estimate of ξ_u, ξ_v

$$\|\xi_u\| + \varepsilon \|\xi_v\| \leq Ch^{k+1},$$

(2.43)

follows from the Gronwall's inequality and the error of the initial condition in Remark 2.6. Combined with the optimal projection error of η_u, η_v, this leads to the optimal error estimate of e_u, e_v in (2.33). □

2.4 Temporal Discretization

In this subsection, we present the fully discrete LDG methods. The implicit midpoint temporal discretization will be used to ensure that the fully discrete methods maintain the mass and energy conserving property. If the energy dissipative method [i.e., $c_u > 0$ or $\widehat{f}$ chosen as (2.12)] is used, the total variation diminishing (TVD) Runge–Kutta method can be used to provide high order accurate temporal approximation.

Let $0 = t_0 < t_1 < \cdots < t_N = T$ be a partition of the interval $[0, T]$ with time step $\Delta t_n = t_{n+1} - t_n$. The following notations

$$u_h^n = u_h(\cdot, t_n), \qquad u_h^{n+\frac{1}{2}} = \frac{1}{2}(u_h^{n+1} + u_h^n), \qquad \delta_t^+ u_h^n = \frac{u_h^{n+1} - u_h^n}{\Delta t_n},$$

are introduced to ease the presentation.

Table 1 The explanation of the numerical methods "C/D-C/D-LDG"

LDG method	Flux $\widehat{f}^{n+\frac{1}{2}}$	Flux $\widehat{(\delta_t^+ v_h^n, (\widehat{u_h})^{n+\frac{1}{2}})}$
C-C-LDG	(2.11)	(2.45) with $c_u = 0$
D-C-LDG	(2.12)	(2.45) with $c_u = 0$
C-D-LDG	(2.11)	(2.45) with $c_u > 0$
D-D-LDG	(2.12)	(2.45) with $c_u > 0$
Central-LDG	(2.11)	$(\{\delta_t^+ v_h^n\}, \{(u_h)^{n+\frac{1}{2}}\})$

The fully discrete implicit midpoint rule with local discontinuous Galerkin scheme takes the following form: we are looking for the solutions u_h^{n+1}, v_h^{n+1}, for $n = 1, 2, \ldots, N - 1$, such that

$$\begin{cases} (\delta_t^+ u_h^n, \phi_1)_j + \varepsilon \mathcal{H}_j^*(\delta_t^+ v_h^n, \phi_1; \widehat{\delta_t^+ v_h^n}) - \mathcal{F}_j^*(u_h^{n+\frac{1}{2}}, \phi_1; \widehat{f}^{n+\frac{1}{2}}) = 0 \\ (v_h^{n+\frac{1}{2}}, \phi_2)_j + \mathcal{H}_j^*(u_h^{n+\frac{1}{2}}, \phi_2; (\widehat{u_h})^{n+\frac{1}{2}}) = 0 \end{cases} \tag{2.44}$$

hold for all test functions ϕ_1, $\phi_2 \in V^k$ on every cell I_j. Here the nonlinear numerical flux $\widehat{f}^{n+\frac{1}{2}} = \widehat{f}(u_h^{n+\frac{1}{2},-}, u_h^{n+\frac{1}{2},+})$ can be chosen as (2.11) or (2.12), and the set of numerical fluxes $(\widehat{\delta_t^+ v_h^n}, (\widehat{u_h})^{n+\frac{1}{2}})$ takes the similar form as (2.9)

$$\begin{cases} \widehat{\delta_t^+ v_h^n} = \delta_t^+ (v_h^*)^n + c_u [u_h^{n+\frac{1}{2}}], \\ (\widehat{u_h})^{n+\frac{1}{2}} = (u_h^*)^{n+\frac{1}{2}}, \end{cases} \tag{2.45}$$

where $c_u \geq 0$ and (u_h^*, v_h^*) can be either $(\cdot^+, \cdot^-)$, $(\cdot^-, \cdot^+)$ or the generalized form in (2.10). Easy to verify that the implicit midpoint rule method is second order accurate in time.

Remark 2.7 Since different choices of the numerical fluxes will be tested in the numerical examples section, we name the fully discrete schemes as "C/D-C/D-LDG", where "C" and "D" stands for "conservative" and "dissipative" respectively, and the detailed explanation can be found in Table 1. The "Central-LDG" method, as explained in Remark 2.1, is also included for comparison. Note that the optimal error estimate proof does not apply to the "Central-LDG" method.

The conservation of continuous mass and energy of the semi-discrete LDG methods are shown in Sect. 2.2. For the fully discrete methods, we have the following results.

Theorem 2.5 *Let u_h^n and v_h^n be the numerical solutions of the fully discrete LDG methods (2.44). With the discrete mass and energy defined as*

$$M_h^n = \int_I u_h^n dx, \qquad E_h^n = \int_I ((u_h^n)^2 + \varepsilon(v_h^n)^2) dx, \tag{2.46}$$

the following mass conservation and energy dissipative property holds

$$M_h^n = M_h^0, \qquad E_h^n \leq E^{n-1} \leq \cdots \leq E_h^0, \tag{2.47}$$

for any n and all the LDG schemes in Table 1. More specifically, C-C-LDG and Central-LDG methods can preserve the energy conservation, that means $E_h^n = E_h^0$.

The proof of this theorem is similar to that of Theorems 2.1 and 2.2, and is omitted here.

Remark 2.8 Note that the implicit midpoint rule method is introduced here, mainly for the purpose of conserving the energy at the discrete level. If one's purpose is to design energy dissipative methods, the explicit TVD Runge-Kutta methods should be used for simplicity.

At the end of this section, we provide some details related to the implementation of the fully discrete methods (2.44). Let U_h be the vectors containing the degree of freedom for the piecewise polynomial solution u_h, and denote $U_h^n = U_h(t_n)$. Similarly, we can define V_h^n. The fully discrete methods (2.44) can be rewritten in the matrix form as

$$
\begin{cases}
AU_h^{n+\frac{1}{2}} + \varepsilon B V_h^{n+\frac{1}{2}} + D_1 V_h^{n+\frac{1}{2}} + \dfrac{\Delta t_n}{2}\left(D_2 U_h^{n+\frac{1}{2}} + f_s\left(U_h^{n+\frac{1}{2}}\right)\right) \\
\qquad = AU_h^n + \varepsilon B V_h^n + D_1 V_h^n, \\
AV_h^{n+\frac{1}{2}} + B U_h^{n+\frac{1}{2}} + D_3 U_h^{n+\frac{1}{2}} = 0,
\end{cases}
\tag{2.48}
$$

where A and B are matrices depending on the polynomial basis functions and the terms $D_1 V_h^{n+\frac{1}{2}}$, $D_2 U_h^{n+\frac{1}{2}}$ and $D_3 U_h^{n+\frac{1}{2}}$ come from the choices of the numerical fluxes $\widehat{\delta_t^+ v_h^n}$, $(\widehat{u_h})^{n+\frac{1}{2}}$. The nonlinear function f_s denotes the discretization of the nonlinear term. The second equation of (2.48) leads to the following relation between V_h and U_h:

$$
V_h^{n+\frac{1}{2}} = K_{uv} U_h^{n+\frac{1}{2}},
\tag{2.49}
$$

where $K_{uv} = -A^{-1}(B + D_3)$. Therefore, the system (2.48) can be reduced to

$$
U_h^{n+\frac{1}{2}} = g_s\left(U_h^{n+\frac{1}{2}}\right) + L\left(U_h^n, V_h^n\right),
\tag{2.50}
$$

where g_s is a nonlinear function and L is a linear function. To solve the nonlinear system (2.50), one could use Newton's method or other iterative methods. A stopping criteria of $\|(U_h^{n+\frac{1}{2}})^{(k)} - (U_h^{n+\frac{1}{2}})^{(k-1)}\| \le \varepsilon$ is used in the numerical implementation, where ε is the control error and is taken as 10^{-15} in our tests. With the solution $U_h^{n+\frac{1}{2}}$ available, one could use (2.49) to evaluate $V_h^{n+\frac{1}{2}}$ if needed.

3 Numerical Experiments of the LDG Methods

In this section, we provide some numerical results of the proposed LDG methods with implicit midpoint rule temporal discretization. When the case $c_u > 0$ is considered in (2.45), we always choose $c_u = 1$ in our tests. We first perform the accuracy tests on the LDG methods to verify the optimal convergence rate. We also test different initial projections and different fluxes, and observe how these affect the order of accuracy. Mass conservation and energy conservation/dissipation property of the proposed methods will also be verified numerically. At the end, the long time behavior of the LDG methods is studied.

3.1 Accuracy Test

The cnoidal-wave solution (1.4), with the following parameters

$$m = 0.9, \quad C = \frac{2m-1}{3m} = 0.2963, \quad D = 0, \quad \varepsilon = 10^{-2}, \quad x_l = 0, \quad x_r = \frac{2K(m)}{B} = 0.9224,$$
(3.1)

is used in this section to check the convergence rate of the proposed LDG methods. The initial conditions $u_0(x)$ is obtained by setting $t = 0$, and the numerical error are computed at the stopping time $T = 1$.

Since the second order implicit midpoint temporal discretizations is employed and our interest is in the effect of various spatial discretizations, we set the time step as $\tau = 0.5877h^2$ (such that $N = 2J^2$). Tables 2, 3, 4, 5, 6 and 7 present the numerical order of accuracy for the LDG methods with P^0, P^1, P^2 and P^3 basis, and with different choices of projections in evaluating the numerical initial conditions.

As seen in Table 2 and Table 4, optimal order of accuracy of u_h and v_h are obtained for both C-C-LDG and D-D-LDG methods, when $(u_h^*, v_{h,t}^*)$ is chosen as $(u_h^+, v_{h,t}^*)$ in fluxes (2.9) and projection π^+ is applied to obtain the initial conditions of u_h. These results agree well with the error estimate in Theorem 2.4. It's worth mentioning that, when L^2 projections is used to obtain the initial conditions of u_h, only kth order accuracy of v_h can be obtained with basis functions in P^k for $k = 1, 2, 3$ for C-C-LDG scheme (see Table 3) and D-D-LDG scheme (see Table 5). In spite of this, optimal order of accuracy of u_h still can be obtained with basis functions in P^k for $k = 1, 2, 3$. The impact of different numerical initial conditions of the LDG methods towards the convergence rate has also been observed by us in [28,29,35]. The performance of the C-D-LDG and D-C-LDG methods is similar and is not presented here to save space. With the other choice of numerical fluxes $(u_h^*, v_{h,t}^*) = (u_h^-, v_{h,t}^+)$, the same numerical results are observed, and are omitted here.

The convergence rate of the Central-LDG method is shown in Table 6. Only kth order accuracy in u_h and v_h are obtained for odd k, which is consistent with our impression that even-odd phenomenon of the central flux. Note that the optimal error estimate result in Theorem 2.4 does not hold for the central flux, as one of the key inequality (2.20) cannot be proven. If the energy dissipative terms are added to the Central-LDG method [i.e., taking $c_u = 1$ and $\widehat{f}$ chosen as (2.12)], the accuracy improves a little for odd k, as seen in Table 7, but optimal convergence still cannot be obtained.

3.2 Mass, Energy Conservation and the Long Time Behavior

In this subsection we study the mass, energy conservation property and the long time behavior of the proposed LDG methods.

We consider the cnoidal-wave solution (1.4) of BBM Eq. (1.1) with the parameters specified in (3.1). First, we plot the time history of the error of mass and energy (i.e., $M_h^N - M_h^0$ and $E_h^N - E_h^0$) of C-C-LDG methods in Fig. 1, with $J = 10$, $T = 250$ and $N = 2480$. Easy to observe that the mass and energy are both exactly preserved by our methods up to the machine error at the level of 10^{-14}.

Figure 2 plots $\|e_u\|$, the time history of L^2 norm of numerical error, of different LDG methods, for the cnoidal-wave example with $J = 10$, $N = 20480$, $T = 30$ and various P^k polynomial basis. We can observe that the L^2 errors of D-C-LDG and D-D-LDG methods are similar and those of C-C-LDG and C-D-LDG methods are similar. The L^2 error of D-D-LDG

Table 2 Numerical error and convergence rates of **C-C-LDG** scheme in the cnoidal-wave example

	h	τ	Error of u				Error of v			
			$\|e_u\|_2$	C_2	$\|e_u\|_\infty$	C_∞	$\|e_v\|_2$	C_2	$\|e_v\|_\infty$	C_∞
P^0	h_1	τ_1	9.7160E−02	*	3.0943E−01	*	1.6709E+00	*	4.8716E+00	*
	$h_1/2$	$\tau_1/4$	3.8744E−02	1.3264	1.3342E−01	1.2136	7.7475E−01	1.1088	3.0440E+00	0.6785
	$h_1/4$	$\tau_1/16$	1.7500E−02	1.1467	5.8275E−02	1.1951	3.5412E−01	1.1295	1.5088E+00	1.0125
	$h_1/8$	$\tau_1/64$	8.4838E−03	1.0446	2.6686E−02	1.1268	1.6724E−01	1.0823	7.3211E−01	1.0433
P^1	h_1	τ_1	1.1716E−02	*	4.9486E−02	*	3.8209E−01	*	1.4150E+00	*
	$h_1/2$	$\tau_1/4$	2.9384E−03	1.9954	1.7444E−02	1.5043	1.0335E−01	1.8864	4.0304E−01	1.8118
	$h_1/4$	$\tau_1/16$	7.4670E−04	1.9764	4.7109E−03	1.8887	2.6360E−02	1.9711	1.0386E−01	1.9563
	$h_1/8$	$\tau_1/64$	1.8859E−04	1.9853	1.2209E−03	1.9481	6.6239E−03	1.9926	2.6135E−02	1.9906
P^2	h_1	τ_1	1.1138E−03	*	7.1263E−03	*	2.3667E−02	*	9.5995E−02	*
	$h_1/2$	$\tau_1/4$	1.4234E−04	2.9680	9.1431E−04	2.9624	2.9189E−03	3.0194	1.0930E−02	3.1347
	$h_1/4$	$\tau_1/16$	1.7910E−05	2.9905	1.1500E−04	2.9910	3.6229E−04	3.0102	1.4507E−03	2.9135
	$h_1/8$	$\tau_1/64$	2.2441E−06	2.9966	1.4112E−05	3.0266	4.5199E−05	3.0028	1.9540E−04	2.8922
P^3	h_1	τ_1	1.0553E−04	*	5.9019E−04	*	2.4803E−03	*	1.4054E−02	*
	$h_1/2$	$\tau_1/4$	6.7539E−06	3.9658	4.8792E−05	3.5965	1.5767E−04	3.9755	7.6858E−04	4.1926
	$h_1/4$	$\tau_1/16$	4.2372E−07	3.9945	3.0825E−06	3.9845	9.9868E−06	3.9808	4.8462E−05	3.9873
	$h_1/8$	$\tau_1/64$	2.6503E−08	3.9989	1.9781E−07	3.9619	6.2631E−07	3.9951	2.9635E−06	4.0315

Projection π^+ for u_0 with $x_l = 0$, $x_r = 0.92237$, $T = 1$, $c_u = 0$, $h_1 = 9.2237E−02$, $\tau_1 = 0.005$

Table 3 Numerical error and convergence rates of **C-C-LDG** scheme in the cnoidal-wave example

	h	τ	Error of u				Error of v			
			$\|e_u\|_2$	C_2	$\|e_u\|_\infty$	C_∞	$\|e_v\|_2$	C_2	$\|e_v\|_\infty$	C_∞
P^0	h_1	τ_1	9.7160E−02	*	3.0943E−01	*	1.6709E+00	*	4.8716E+00	*
	$h_1/2$	$\tau_1/4$	3.8744E−02	1.3264	1.3342E−01	1.2136	7.7475E−01	1.1088	3.0440E+00	0.6785
	$h_1/4$	$\tau_1/16$	1.7500E−02	1.1467	5.8275E−02	1.1951	3.5412E−01	1.1295	1.5088E+00	1.0125
	$h_1/8$	$\tau_1/64$	8.4838E−03	1.0446	2.6686E−02	1.1268	1.6724E−01	1.0823	7.3211E−01	1.0433
P^1	h_1	τ_1	1.6107E−02	*	6.7886E−02	*	6.3332E−01	*	2.7165E+00	*
	$h_1/2$	$\tau_1/4$	4.3180E−03	1.8992	1.9815E−02	1.7765	3.2547E−01	0.9604	1.4720E+00	0.8840
	$h_1/4$	$\tau_1/16$	1.0974E−03	1.9763	5.3724E−03	1.8829	1.6122E−01	1.0134	7.2349E−01	1.0248
	$h_1/8$	$\tau_1/64$	2.7531E−04	1.9949	1.3803E−03	1.9606	7.9684E−02	1.0167	3.5379E−01	1.0321
P^2	h_1	τ_1	1.4699E−03	*	7.3882E−03	*	9.1552E−02	*	4.8003E−01	*
	$h_1/2$	$\tau_1/4$	1.7952E−04	3.0335	9.5098E−04	2.9577	1.9902E−02	2.2017	1.0917E−01	2.1365
	$h_1/4$	$\tau_1/16$	2.2848E−05	2.9740	1.1492E−04	3.0488	4.7120E−03	2.0785	2.2904E−02	2.2530
	$h_1/8$	$\tau_1/64$	2.9075E−06	2.9743	1.4249E−05	3.0116	1.1598E−03	2.0224	5.0858E−03	2.1710
P^3	h_1	τ_1	1.1841E−04	*	5.7533E−04	*	1.2012E−02	*	6.5509E−02	*
	$h_1/2$	$\tau_1/4$	7.9288E−06	3.9006	4.8275E−05	3.5751	1.7401E−03	2.7872	1.2167E−02	2.4287
	$h_1/4$	$\tau_1/16$	5.0308E−07	3.9782	3.0759E−06	3.9722	2.2553E−04	2.9478	1.6642E−03	2.8701
	$h_1/8$	$\tau_1/64$	3.1542E−08	3.9954	1.9666E−07	3.9672	2.8465E−05	2.9861	2.1238E−04	2.9701

L^2 **Projection** π for u_0 with $x_l = 0$, $x_r = 0.92237$, $T = 1$, $c_u = 0$, $h_1 = 9.2237E{-}02$, $\tau_1 = 0.005$

Table 4 Numerical error and convergence rates of **D-D-LDG** scheme in the cnoidal-wave example

h	τ	Error of u				Error of v			
		$\|e_u\|_2$	C_2	$\|e_u\|_\infty$	C_∞	$\|e_v\|_2$	C_2	$\|e_v\|_\infty$	C_∞
P^0									
h_1	τ_1	2.0424E−01	*	4.1735E−01	*	1.8676E+00	*	4.4284E+00	*
$h_1/2$	$\tau_1/4$	1.2945E−01	0.6579	2.7717E−01	0.5905	1.2367E+00	0.5947	3.0423E+00	0.5416
$h_1/4$	$\tau_1/16$	7.4304E−02	0.8008	1.5995E−01	0.7931	7.2654E−01	0.7674	1.9181E+00	0.6654
$h_1/8$	$\tau_1/64$	3.9987E−02	0.8939	8.7333E−02	0.8730	3.9509E−01	0.8788	1.0671E+00	0.8460
P^1									
h_1	τ_1	1.3748E−02	*	3.7081E−02	*	4.6783E−01	*	1.6268E+00	*
$h_1/2$	$\tau_1/4$	3.1579E−03	2.1222	1.4263E−02	1.3784	1.6801E−01	1.4774	6.2029E−01	1.3910
$h_1/4$	$\tau_1/16$	7.6045E−04	2.0540	4.2235E−03	1.7557	4.9796E−02	1.7545	1.8564E−01	1.7404
$h_1/8$	$\tau_1/64$	1.8891E−04	2.0092	1.1582E−03	1.8665	1.3476E−02	1.8857	5.0545E−02	1.8769
P^2									
h_1	τ_1	1.2229E−03	*	7.2262E−03	*	4.0985E−02	*	1.6067E−01	*
$h_1/2$	$\tau_1/4$	1.4790E−04	3.0476	9.2629E−04	2.9637	5.5841E−03	2.8757	2.0425E−02	2.9757
$h_1/4$	$\tau_1/16$	1.8144E−05	3.0271	1.1816E−04	2.9707	7.2667E−04	2.9420	2.9659E−03	2.7838
$h_1/8$	$\tau_1/64$	2.2538E−06	3.0090	1.4389E−05	3.0377	9.2972E−05	2.9664	4.0726E−04	2.8644
P^3									
h_1	τ_1	1.1052E−04	*	5.9263E−04	*	3.4501E−03	*	1.9206E−02	*
$h_1/2$	$\tau_1/4$	6.8793E−06	4.0059	4.7618E−05	3.6376	2.5237E−04	3.7730	1.2621E−03	3.9276
$h_1/4$	$\tau_1/16$	4.2660E−07	4.0113	3.0223E−06	3.9778	1.7008E−05	3.8913	8.2418E−05	3.9368
$h_1/8$	$\tau_1/64$	2.6570E−08	4.0050	1.9635E−07	3.9442	1.0993E−06	3.9515	5.1729E−06	3.9939

Projection π^+ for u_0 with $x_l = 0$, $x_r = 0.92237$, $T = 1$, $c_u = 1$, $h_1 = 9.2237E−02$, $\tau_1 = 0.005$

Table 5 Numerical error and convergence rates of **D-D-LDG** scheme in the cnoidal-wave example

h	τ	Error of u				Error of v			
		$\|e_u\|_2$	C_2	$\|e_u\|_\infty$	C_∞	$\|e_v\|_2$	C_2	$\|e_v\|_\infty$	C_∞
P^0									
h_1	τ_1	2.0424E−01	*	4.1735E−01	*	1.8676E+00	*	4.4284E+00	*
$h_1/2$	$\tau_1/4$	1.2945E−01	0.6579	2.7717E−01	0.5905	1.2367E+00	0.5947	3.0423E+00	0.5416
$h_1/4$	$\tau_1/16$	7.4304E−02	0.8008	1.5995E−01	0.7931	7.2654E−01	0.7674	1.9181E+00	0.6654
$h_1/8$	$\tau_1/64$	3.9987E−02	0.8939	8.7333E−02	0.8730	3.9509E−01	0.8788	1.0671E+00	0.8460
P^1									
h_1	τ_1	1.5261E−02	*	3.9497E−02	*	5.2915E−01	*	1.3911E+00	*
$h_1/2$	$\tau_1/4$	3.8950E−03	1.9701	1.5692E−02	1.3317	2.7051E−01	0.9680	1.0491E+00	0.4070
$h_1/4$	$\tau_1/16$	1.0209E−03	1.9318	4.7062E−03	1.7374	1.4141E−01	0.9358	6.1285E−01	0.7756
$h_1/8$	$\tau_1/64$	2.6427E−04	1.9498	1.2979E−03	1.8583	7.3811E−02	0.9380	3.2630E−01	0.9093
P^2									
h_1	τ_1	1.4532E−03	*	7.2981E−03	*	8.8339E−02	*	4.1731E−01	*
$h_1/2$	$\tau_1/4$	1.8135E−04	3.0024	9.3930E−04	2.9579	2.0434E−02	2.1121	1.1070E−01	1.9144
$h_1/4$	$\tau_1/16$	2.2967E−05	2.9812	1.1725E−04	3.0020	4.7922E−03	2.0922	2.3727E−02	2.2221
$h_1/8$	$\tau_1/64$	2.9122E−06	2.9794	1.4297E−05	3.0358	1.1667E−03	2.0382	5.2081E−03	2.1877
P^3									
h_1	τ_1	1.2290E−04	*	5.8517E−04	*	1.0858E−02	*	5.2026E−02	*
$h_1/2$	$\tau_1/4$	7.8249E−06	3.9732	4.7357E−05	3.6272	1.5674E−03	2.7924	1.0876E−02	2.2580
$h_1/4$	$\tau_1/16$	4.9446E−07	3.9841	3.0205E−06	3.9707	2.1194E−04	2.8866	1.5749E−03	2.7879
$h_1/8$	$\tau_1/64$	3.1190E−08	3.9867	1.9537E−07	3.9505	2.7554E−05	2.9434	2.0668E−04	2.9298

L^2 **Projection** π for u_0 with $x_l = 0$, $x_r = 0.92237$, $T = 1$, $c_u = 1$, $h_1 = 9.2237E{-}02$, $\tau_1 = 0.005$

Table 6 Numerical error and convergence rates of **Central-LDG** scheme in the cnoidal-wave example

h	τ	Error of u				Error of v			
		$\|e_u\|_2$	C_2	$\|e_u\|_\infty$	C_∞	$\|e_v\|_2$	C_2	$\|e_v\|_\infty$	C_∞
P^0									
h_1	τ_1	8.7143E−02	*	2.7492E−01	*	7.1599E−01	*	2.6373E+00	*
$h_1/2$	$\tau_1/4$	3.6716E−02	1.2470	1.1893E−01	1.2089	3.4142E−01	1.0684	1.3535E+00	0.9624
$h_1/4$	$\tau_1/16$	1.7182E−02	1.0955	5.3281E−02	1.1584	1.6058E−01	1.0883	6.9529E−01	0.9610
$h_1/8$	$\tau_1/64$	8.4417E−03	1.0253	2.5384E−02	1.0697	7.8908E−02	1.0251	3.4381E−01	1.0160
P^1									
h_1	τ_1	6.2266E−02	*	1.8843E−01	*	5.9816E−01	*	2.1726E+00	*
$h_1/2$	$\tau_1/4$	3.0568E−02	1.0264	9.2727E−02	1.0229	3.3391E−01	0.8411	1.4077E+00	0.6261
$h_1/4$	$\tau_1/16$	1.5194E−02	1.0085	4.6762E−02	0.9877	1.7244E−01	0.9533	7.5429E−01	0.9001
$h_1/8$	$\tau_1/64$	7.5853E−03	1.0023	2.3289E−02	1.0057	8.6954E−02	0.9878	3.8277E−01	0.9786
P^2									
h_1	τ_1	1.9011E−03	*	8.3263E−03	*	7.3126E−02	*	3.6532E−01	*
$h_1/2$	$\tau_1/4$	1.0744E−04	4.1452	4.9743E−04	4.0651	6.9139E−03	3.4028	4.4030E−02	3.0526
$h_1/4$	$\tau_1/16$	1.1991E−05	3.1635	5.4064E−05	3.2018	7.9974E−04	3.1119	4.5490E−03	3.2749
$h_1/8$	$\tau_1/64$	1.4627E−06	3.0353	6.5786E−06	3.0388	9.7671E−05	3.0335	5.1069E−04	3.1550
P^3									
h_1	τ_1	3.3894E−04	*	1.2296E−03	*	9.7583E−03	*	5.3283E−02	*
$h_1/2$	$\tau_1/4$	4.2412E−05	2.9985	1.5029E−04	3.0323	1.6248E−03	2.5863	9.9913E−03	2.4149
$h_1/4$	$\tau_1/16$	5.3080E−06	2.9982	1.8424E−05	3.0281	2.2077E−04	2.8796	1.3638E−03	2.8731
$h_1/8$	$\tau_1/64$	6.6370E−07	2.9996	2.2559E−06	3.0298	2.8209E−05	2.9683	1.7573E−04	2.9562

L^2 **Projection** π for u_0 with $x_l = 0$, $x_r = 0.92237$, $T = 1$, $c_u = 0$, $h_1 = 9.2237E−02$, $\tau_1 = 1.5625E−03$

Table 7 Numerical error and convergence orders of u and v of **Central-LDG scheme with dissipative term added** in the cnoidal-wave example

h	τ	Error of u				Error of v			
		$\|e_u\|_2$	C_2	$\|e_u\|_\infty$	C_∞	$\|e_v\|_2$	C_2	$\|e_v\|_\infty$	C_∞
P^0									
h_1	τ_1	2.0766E−01	*	4.1851E−01	*	1.7751E+00	*	3.8720E+00	*
$h_1/2$	$\tau_1/4$	1.3101E−01	0.6645	2.7938E−01	0.5830	1.1746E+00	0.5957	2.6950E+00	0.5228
$h_1/4$	$\tau_1/16$	7.4530E−02	0.8138	1.6175E−01	0.7884	6.8559E−01	0.7767	1.6328E+00	0.7229
$h_1/8$	$\tau_1/64$	3.9963E−02	0.8992	8.7398E−02	0.8881	3.7301E−01	0.8781	9.1864E−01	0.8298
P^1									
h_1	τ_1	2.3762E−02	*	6.3362E−02	*	4.7793E−01	*	1.4827E+00	*
$h_1/2$	$\tau_1/4$	7.8784E−03	1.5927	2.0562E−02	1.6236	2.6290E−01	0.8623	1.0157E+00	0.5458
$h_1/4$	$\tau_1/16$	2.3444E−03	1.7487	6.4632E−03	1.6697	1.4220E−01	0.8866	5.9815E−01	0.7639
$h_1/8$	$\tau_1/64$	6.7319E−04	1.8002	1.9583E−03	1.7227	7.5500E−02	0.9134	3.2807E−01	0.8665
P^2									
h_1	τ_1	1.5408E−03	*	5.1832E−03	*	5.8124E−02	*	2.7839E−01	*
$h_1/2$	$\tau_1/4$	1.0888E−04	3.8228	5.2111E−04	3.3142	7.2635E−03	3.0004	5.0099E−02	2.4743
$h_1/4$	$\tau_1/16$	1.2066E−05	3.1738	5.5886E−05	3.2210	9.0691E−04	3.0016	6.0832E−03	3.0419
$h_1/8$	$\tau_1/64$	1.4653E−06	3.0417	6.7028E−06	3.0597	1.1306E−04	3.0039	7.2839E−04	3.0621
P^3									
h_1	τ_1	1.4128E−04	*	5.1391E−04	*	8.6155E−03	*	4.6781E−02	*
$h_1/2$	$\tau_1/4$	1.5211E−05	3.2154	6.6286E−05	2.9547	1.2930E−03	2.7362	7.3664E−03	2.6669
$h_1/4$	$\tau_1/16$	1.5633E−06	3.2824	5.8815E−06	3.4945	1.6906E−04	2.9351	7.2817E−04	3.3386
$h_1/8$	$\tau_1/64$	1.6626E−07	3.2331	5.6284E−07	3.3854	2.3327E−05	2.8575	8.5507E−05	3.0902

L^2 **Projection** π for u_0 with $x_l = 0$, $x_r = 0.92237$, $T = 1$, $c_u = 1$, $h_1 = 9.2237E-02$, $\tau_1 = 1.5625E-03$
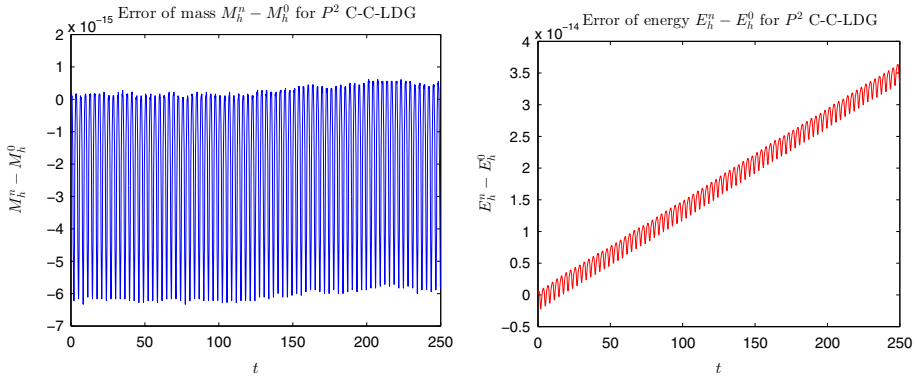
Fig. 1 Errors of mass (left) and energy (right) of C-C-LDG scheme in Sect. 3.2, with $J = 10$, $T = 250$, $N = 2480$ and P^2 polynomial basis
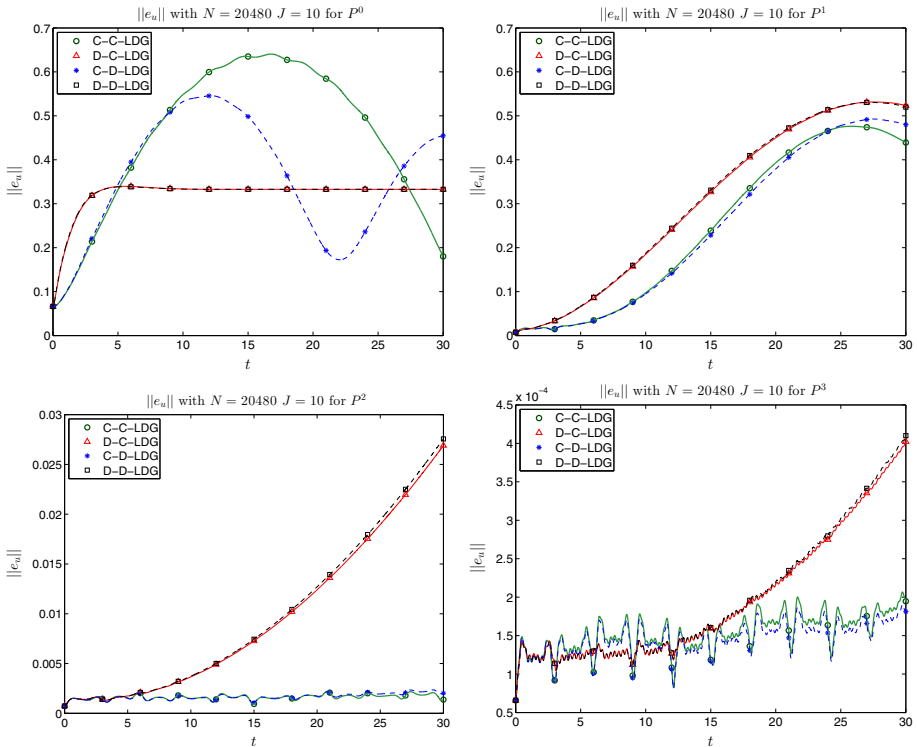

Fig. 2 Time history of the numerical errors of u_h in L^2 norm with $J = 10$, $N = 20,480$ and $T = 30$ of C-C-LDG, C-D-LDG, D-C-LDG and D-D-LDG methods in Sect. 3.2, with P^0 (top left), P^1 (top right), P^2 (bottom left) and P^3 (bottom right) polynomial basis

is growing faster than C-C-LDG method. This means that the influence of term $c_u[u_h]$ in flux $\widehat{v_{h,t}}$ is not as obvious as the nonlinear term flux $\widehat{f}$, and in general, the conserved C-C-LDG scheme performs better. From the bottom of Fig. 2, we can see the the errors of the C-C-LDG scheme do not grow significantly in time due to the energy conserving property.

Next we focus on C-C-LDG and D-D-LDG methods, and provide a thorough comparison of them by Figs. 3, 4 and 5 with the explanations below. In the top of Fig. 3, we show the time history of the numerical errors of u_h in L^∞ norm with uniform time steps $\tau = 0.0323$ (top left), $\tau = 0.0161$ (top right) and P^0 polynomial basis. It can be observed that the errors of different time step sizes are similar, which means the numerical error is dominated by the spatial discretization. Also, the numerical error of energy conserving scheme is smaller. The middle and bottom of Fig. 3 provide the comparison of numerical solutions with the exact solution at different stopping times, and the time history of $u(x_m, t)$ with $x_m = (x_l + x_r)/2$, uniform spatial cells $J = 40$ and the time step $\tau = 0.161$. It is very easy to observe that, the D-D-LDG scheme has a larger phase error, which makes the solution very inaccurate in the long time simulation. On the other hand, C-C-LDG scheme demonstrate a good approximation to the exact solution. When P^2 and P^3 polynomial basis are used, the same numerical results can be observed in Figs. 4 and 5, respectively. The C-C-LDG scheme demonstrates a better approximation to the exact solution than the D-D-LDG scheme. In addition, we can see the difference between C-C-LDG and D-D-LDG becomes less obvious, as the polynomial degree k increases.

Figure 6 shows the comparison of the waveform of C-C-LDG and D-D-LDG methods at different times $T = 70, 200, 250$ and 290. Significant phase error can be observed for the D-D-LDG methods, while the C-C-LDG methods can capture the wave well. At time $T = 290$, the solution of D-D-LDG methods seems to match well with the exact solution, but this is because the phase error has accumulated and the wave is now one period behind (with periodic boundary condition used). Also, the magnitude of the numerical solution of the C-C-LDG scheme (red line) stays as 1, while the amplitude of D-D-LDG result (blue line) decreases gradually over time.

In [31], energy conserving LDG method for the Camassa–Holm equation is investigated and tested. One question about [31, Figure 2] remains unanswered in that paper. A smaller phase error of the energy conserving methods was observed for that numerical test, but the improvement in terms of the phase error is not as good as that for the KdV [24] and Degasperis-Procesi [32] equations. We revisited this issue for this simpler BBM equation. Figure 7, the left column, reproduces similar observation as in [31, Figure 2], and one can observe obvious phase error of both C-C-LDG and D-D-LDG methods, although C-C-LDG method has a smaller phase error. The right column of Fig. 7 provide the numerical results with a half time step size while keeping all the other parameters. After reducing Δt, the numerical error of energy conserving C-C-LDG methods decreases significantly, leading to a much smaller phase error, but the error of the energy dissipative D-D-LDG methods does not change much. Therefore, the large phase error of energy conserving methods in Fig. 7 (the left column) is mainly due to the temporal discretization error.

3.3 Non-uniform Meshes

In this subsection, numerical results of the proposed methods on non-uniform spatial meshes are provided. Both the accuracy and long time behavior are tested. The non-uniform meshes are taken of the style $\{h, 2h, 3h, h, 2h, 3h, \ldots\}$, and J again stands for the total number of cells.

We consider the cnoidal-wave solution (1.4) of BBM Eq. (1.1) with the parameters specified in (3.1). In the first accuracy test, we set the time step as $\tau = 2.3508h^2$ (such that $N = 2J^2$). $(u_h^*, v_{h,t}^*)$ is chosen as $(u_h^+, v_{h,t}^-)$ in the fluxes (2.9), and projection π^+ is applied to obtain the initial conditions of u_h. Tables 8 and 9 present the accuracy test of C-C-LDG and
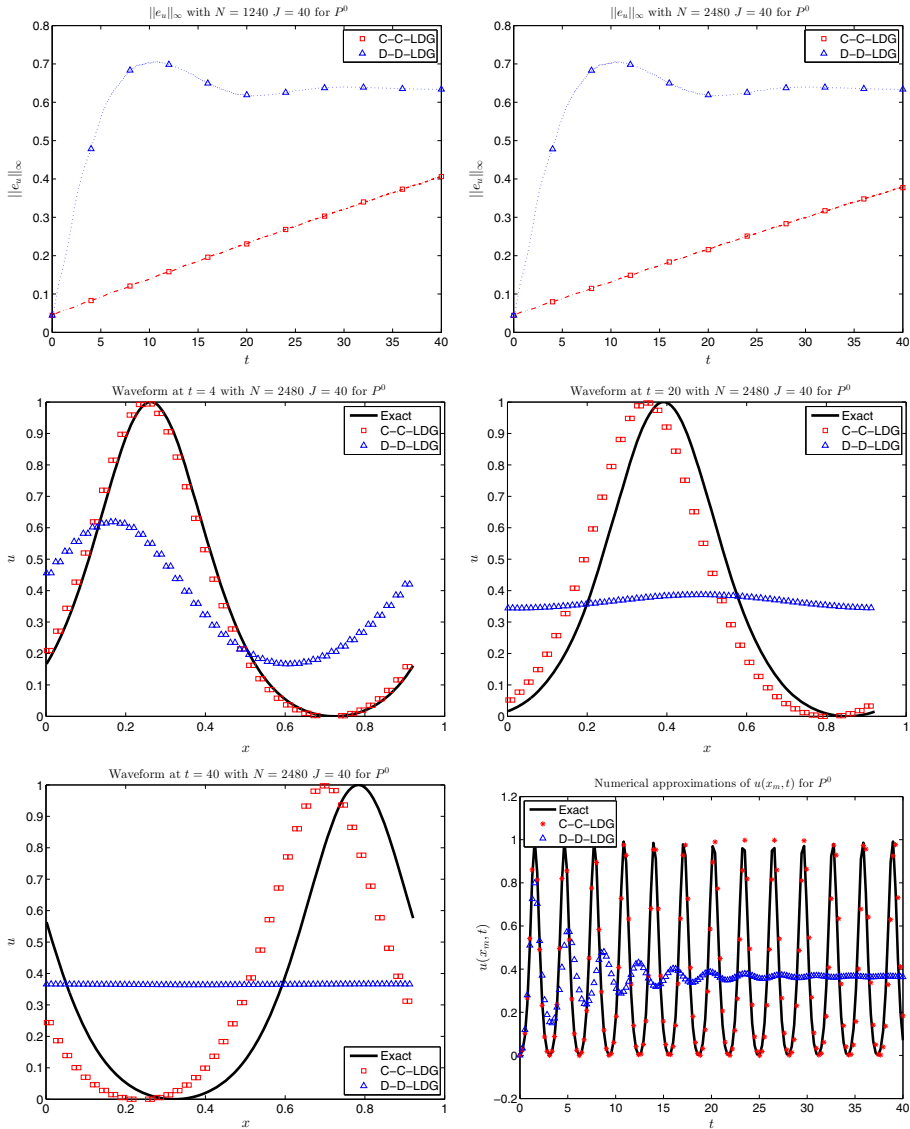
Fig. 3 Time history of the numerical errors of u_h in L^∞ norm with uniform time cells $N = 1240$ (top left) and 2480 (top right) at $t = 40$, waveform at $t = 4$ (middle left), $t = 20$ (middle right) and $t = 40$ (bottom left) and time history of $u(x_m, t)$ (bottom right) of C-C-LDG and D-D-LDG methods in the cnoidal-wave example with uniform spatial cells $J = 40$, $x_m = (x_l + x_r)/2$ and P^0 polynomial basis

D-D-LDG methods on non-uniform meshes, respectively. We can observe that both methods demonstrate an optimal order of convergence rate on u_h and v_h.

Both C-C-LDG and D-D-LDG methods are simulated for this cnoidal-wave example, on non-uniform meshes using P^0 (with $J = 40$) and P^3 (with $J = 10$) polynomial basis. Figure 8 shows the time history of their numerical errors of u_h in L^∞ norm. Comparing with the top right of Figs. 3 and 5, we observe that non-uniform spatial meshes lead to
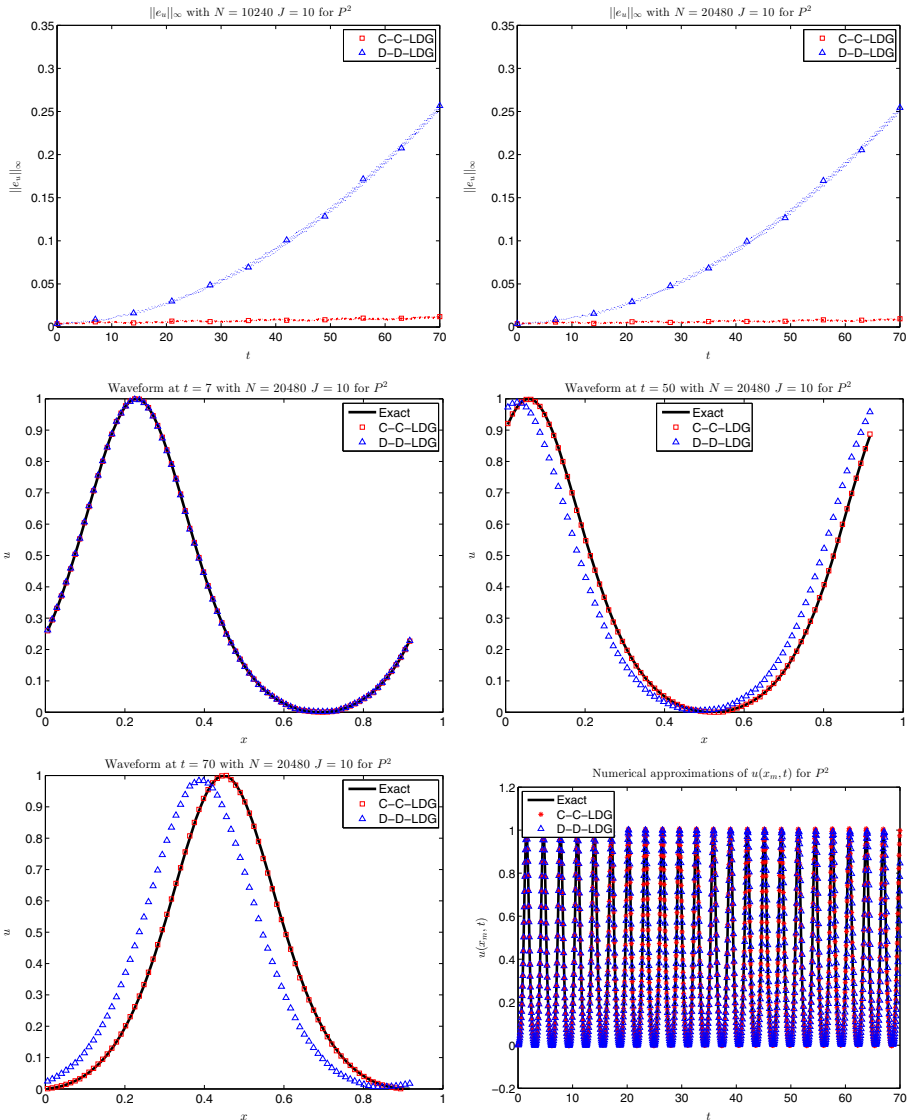
Fig. 4 Time history of the numerical errors of u_h in L^∞ norm with uniform time cells $N = 10{,}240$ (top left) and $N = 20{,}480$ (top right) for $T = 70$, waveform at $t = 7$ (middle left), $t = 50$ (middle right) and $t = 70$ (bottom left) and time history of $u(x_m, t)$ (bottom right) of C-C-LDG and D-D-LDG methods in the cnoidal-wave example with uniform spatial cells $J = 10$, $x_m = (x_l + x_r)/2$ and P^2 polynomial basis

larger numerical error with the same J, and the C-C-LDG scheme demonstrates a better approximation to the exact solution than the D-D-LDG scheme.

Figure 9 shows the comparison of the waveform of C-C-LDG and D-D-LDG methods at different times $T = 50, 100, 140$ and 150, on non-uniform meshes ($J = 10$) for P^2 polynomial basis. We can obtain the same conclusion as observed in Fig. 6 for the tests with uniform meshes, namely the C-C-LDG methods have smaller phase and amplitude error than
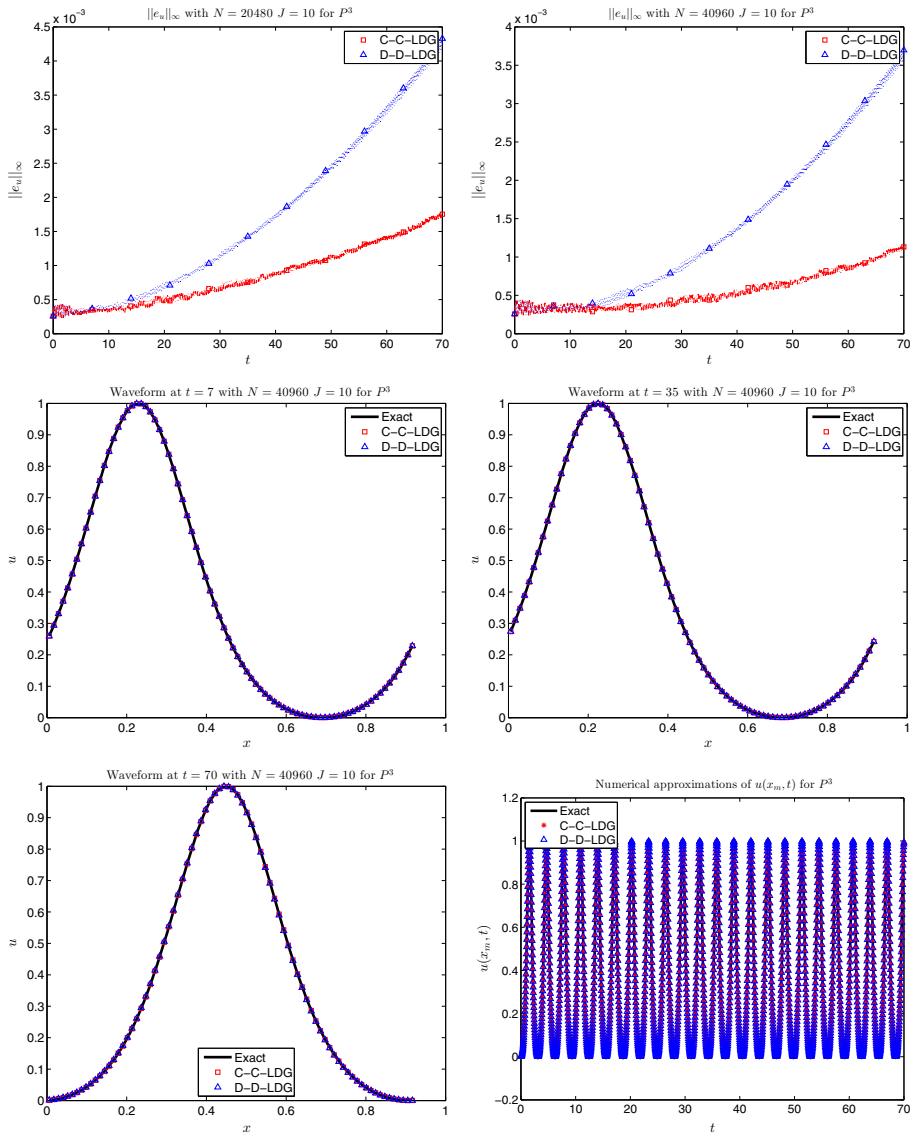
Fig. 5 Time history of the numerical errors of u_h in L^∞ norm with uniform time cells $N = 20,480$ (top left) and $N = 40,960$ (top right) for $T = 70$, waveform at $t = 7$ (middle left), $t = 50$ (middle right) and $t = 70$ (bottom left) and time history of $u(x_m, t)$ (bottom right) of C-C-LDG and D-D-LDG methods in the cnoidal-wave example with uniform spatial cells $J = 10$, $x_m = (x_l + x_r)/2$ and P^3 polynomial basis

D-D-LDG methods. Comparing with Fig. 6, we can observe, under non-uniform meshes, the phase error of the D-D-LDG methods accumulates faster: the peak of the wave lag one period behind around $t = 150$, while the same phenomenon occurs around $t = 290$ with uniform spatial meshes.
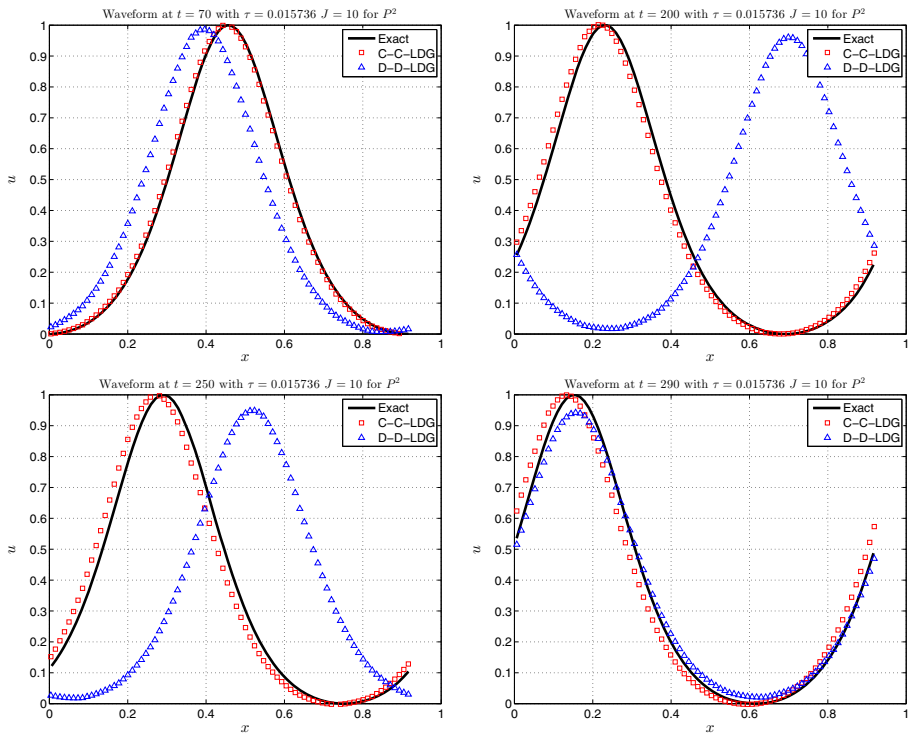
Fig. 6 The comparison of the waveform of C-C-LDG and D-D-LDG methods at different times $t = 70, 200, 250, 290$ in the cnoidal-wave example with uniform spatial cells $J = 10$, $\tau = 0.015736$ and P^2 polynomial basis

4 Energy Conserving LDG Method Via Doubling-the-Unknowns

Optimal energy conserving DG methods have been presented for linear symmetric hyperbolic systems by Fu and Shu in [36], based on the doubling-the-unknowns idea to introduce an auxiliary zero unknown equation. The same idea has been extended in [37] to provide an energy conserving ultra-weak DG method for the KdV equation, where comparison with existing energy conserving or dissipative DG methods have been provided to demonstrate the better performance of this optimal energy conserving DG method. In this section, we will extend the same idea to the BBM equation to derive and analyze optimal energy conserving LDG method with double unknowns (named as dLDG), and the main focus is two-folds: first, we want to show that the suboptimal Central-LDG method can be extended to be optimal in this framework; second, the comparison of dLDG methods with the energy conserving methods presented in Sect. 2 will be presented.

We start by doubling the unknown functions with the introduction of an auxiliary zero function $g(x, t)$, and consider the following system

$$
\begin{cases}
u_t - \varepsilon u_{xxt} + u u_x = 0, \\
g_t - \varepsilon g_{xxt} = 0,
\end{cases}
\tag{4.1}
$$
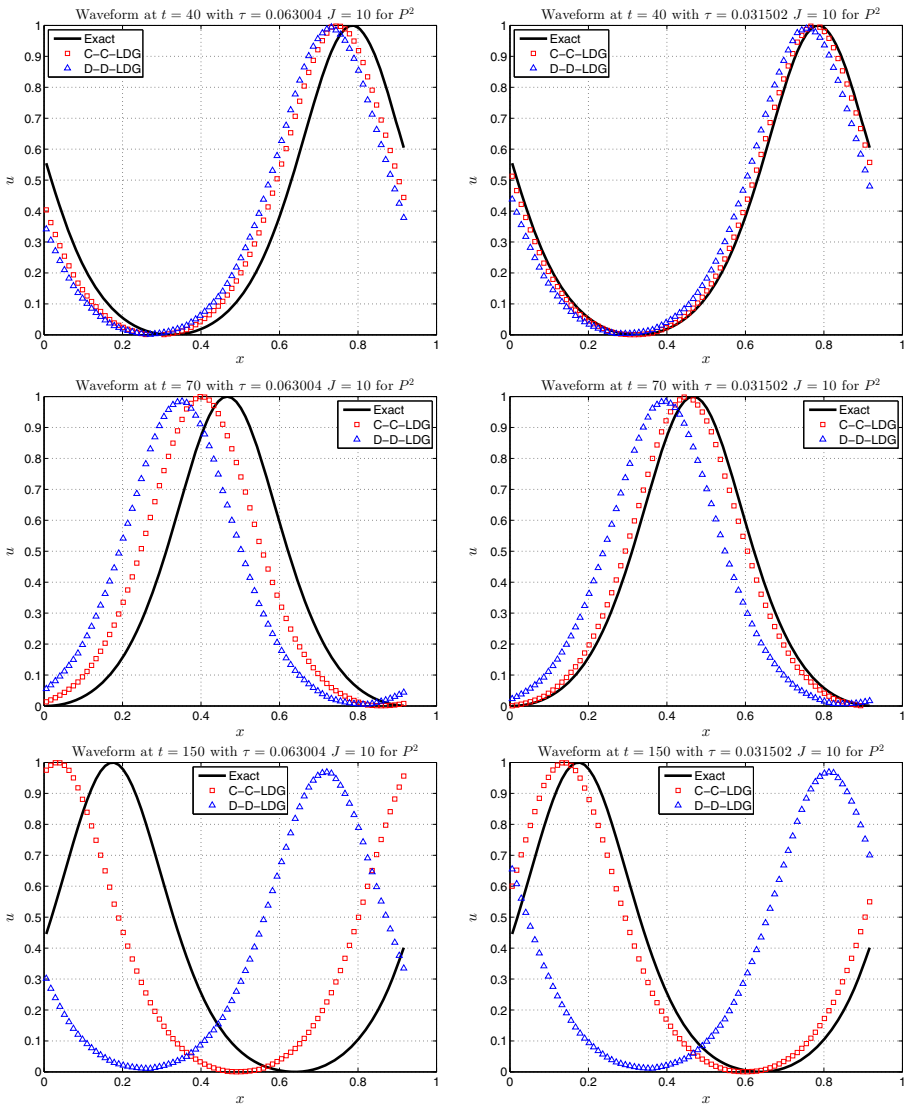
Fig. 7 The comparison of the waveform of C-C-LDG and D-D-LDG methods at different times $t = 40$ (top), $t = 70$ (middle), $t = 150$ (bottom) with time step $\tau = 0.063004$ (left) and $\tau = 0.031502$ (right), in the cnoidal-wave example with uniform spatial cells $J = 10$ and P^2 polynomial basis

with initial condition $u(x, 0) = u_0(x)$ and $g(x, 0) = 0$. As explained in [37], one could add the nonlinear term gg_x to the second equation to obtain the dLDG method, but it is not found to be beneficial, therefore, to save computational cost, this nonlinear term is not included. Analytically, $g(x, t)$ should stay as 0 for any t, but this will not be the case numerically, due to our choice of the numerical fluxes to couple u and g togther.

Table 8 Accuracy test on non-uniform meshes: numerical error and convergence rates of **C-C-LDG** scheme in the cnoidal-wave example

h	τ	Error of u				Error of v			
		$\|e_u\|_2$	C_2	$\|e_u\|_\infty$	C_∞	$\|e_v\|_2$	C_2	$\|e_v\|_\infty$	C_∞
P^0									
h_1	τ_1	4.4655E−02	*	1.6811E−01	*	4.2819E−01	*	1.4257E+00	*
$h_1/2$	$\tau_1/4$	2.4834E−02	0.8465	9.2487E−02	0.8621	2.0879E−01	1.0362	8.2261E−01	0.7934
$h_1/4$	$\tau_1/16$	1.3065E−02	0.9266	4.8150E−02	0.9417	1.0353E−01	1.0119	4.3659E−01	0.9139
$h_1/8$	$\tau_1/64$	6.6932E−03	0.9649	2.4409E−02	0.9801	5.1651E−02	1.0032	2.2346E−01	0.9663
P^1									
h_1	τ_1	2.2941E−03	*	1.6439E−02	*	7.6537E−02	*	3.4387E−01	*
$h_1/2$	$\tau_1/4$	5.6788E−04	2.0143	4.5342E−03	1.8582	1.9774E−02	1.9526	9.5951E−02	1.8415
$h_1/4$	$\tau_1/16$	1.4245E−04	1.9951	1.2064E−03	1.9101	4.9860E−03	1.9876	2.5322E−02	1.9219
$h_1/8$	$\tau_1/64$	3.5746E−05	1.9946	3.0769E−04	1.9712	1.2492E−03	1.9969	6.4263E−03	1.9783
P^2									
h_1	τ_1	1.0288E−04	*	8.1468E−04	*	2.1485E−03	*	9.8155E−03	*
$h_1/2$	$\tau_1/4$	1.3033E−05	2.9807	1.1445E−04	2.8315	2.6359E−04	3.0270	1.4553E−03	2.7538
$h_1/4$	$\tau_1/16$	1.6330E−06	2.9966	1.3958E−05	3.0355	3.2889E−05	3.0027	1.9606E−04	2.8919
$h_1/8$	$\tau_1/64$	2.0433E−07	2.9986	1.7580E−06	2.9891	4.1091E−06	3.0007	2.5248E−05	2.9571
P^3									
h_1	τ_1	4.9308E−06	*	4.6713E−05	*	1.0688E−04	*	6.4172E−04	*
$h_1/2$	$\tau_1/4$	3.0075E−07	4.0352	2.9424E−06	3.9888	7.1420E−06	3.9035	4.8008E−05	3.7406
$h_1/4$	$\tau_1/16$	1.8811E−08	3.9989	1.9577E−07	3.9098	4.4789E−07	3.9951	2.9366E−06	4.0310
$h_1/8$	$\tau_1/64$	1.1757E−09	4.0000	1.2377E−08	3.9835	2.8017E−08	3.9988	1.8064E−07	4.0230

Projection π^+ for u_0 with $x_l = 0$, $x_r = 0.92237$, $T = 1$, $c_u = 0$, $h_1 = 1.5373E{-}02$, $\tau_1 = 5.5556E{-}04$

Table 9 Accuracy test on non-uniform meshes: numerical error and convergence rates of **D-D-LDG** scheme in the cnoidal-wave example

	h	τ	Error of u				Error of v			
			$\|e_u\|_2$	C_2	$\|e_u\|_\infty$	C_∞	$\|e_v\|_2$	C_2	$\|e_v\|_\infty$	C_∞
P^0	h_1	τ_1	1.0129E−01	*	2.3797E−01	*	1.0728E+00	*	2.5646E+00	*
	$h_1/2$	$\tau_1/4$	5.7632E−02	0.8136	1.5151E−01	0.6514	6.4231E−01	0.7400	1.6538E+00	0.6329
	$h_1/4$	$\tau_1/16$	3.0825E−02	0.9028	8.3809E−02	0.8542	3.5215E−01	0.8671	9.6249E−01	0.7810
	$h_1/8$	$\tau_1/64$	1.5940E−02	0.9515	4.3821E−02	0.9355	1.8423E−01	0.9347	5.2673E−01	0.8697
P^1	h_1	τ_1	2.5607E−03	*	1.3127E−02	*	1.2846E−01	*	5.5514E−01	*
	$h_1/2$	$\tau_1/4$	5.9035E−04	2.1169	4.2188E−03	1.6377	3.7714E−02	1.7681	1.7399E−01	1.6739
	$h_1/4$	$\tau_1/16$	1.4363E−04	2.0393	1.1568E−03	1.8666	1.0181E−02	1.8892	4.9245E−02	1.8209
	$h_1/8$	$\tau_1/64$	3.5760E−05	2.0059	3.0085E−04	1.9431	2.6401E−03	1.9472	1.2971E−02	1.9247
P^2	h_1	τ_1	1.0703E−04	*	7.9871E−04	*	4.0733E−03	*	2.0756E−02	*
	$h_1/2$	$\tau_1/4$	1.3199E−05	3.0194	1.1729E−04	2.7676	5.2919E−04	2.9444	2.9716E−03	2.8042
	$h_1/4$	$\tau_1/16$	1.6399E−06	3.0088	1.4144E−05	3.0518	6.7684E−05	2.9669	4.0887E−04	2.8615
	$h_1/8$	$\tau_1/64$	2.0464E−07	3.0025	1.7736E−06	2.9954	8.5684E−06	2.9817	5.3339E−05	2.9384
P^3	h_1	τ_1	5.0128E−06	*	4.4567E−05	*	1.7905E−04	*	1.1661E−03	*
	$h_1/2$	$\tau_1/4$	3.0280E−07	4.0492	2.9307E−06	3.9267	1.2183E−05	3.8775	8.1962E−05	3.8305
	$h_1/4$	$\tau_1/16$	1.8859E−08	4.0050	1.9483E−07	3.9110	7.8721E−07	3.9520	5.1286E−06	3.9983
	$h_1/8$	$\tau_1/64$	1.1769E−09	4.0021	1.2338E−08	3.9810	4.9962E−08	3.9778	3.2121E−07	3.9970

Projection π^+ for u_0 with $x_l = 0$, $x_r = 0.92237$, $T = 1$, $c_u = 1$, $h_1 = 1.5373E\text{-}02$, $\tau_1 = 5.5556E\text{-}04$
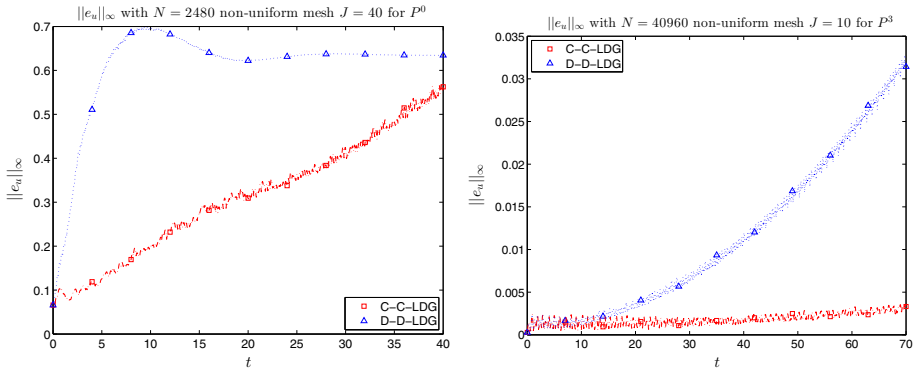
Fig. 8 Non-uniform meshes: time history of the numerical errors of u_h in L^∞ norm of C-C-LDG and D-D-LDG methods on non-uniform meshes, using P^0 (left, $J = 40$) and P^3 (right, $J = 10$) polynomial basis
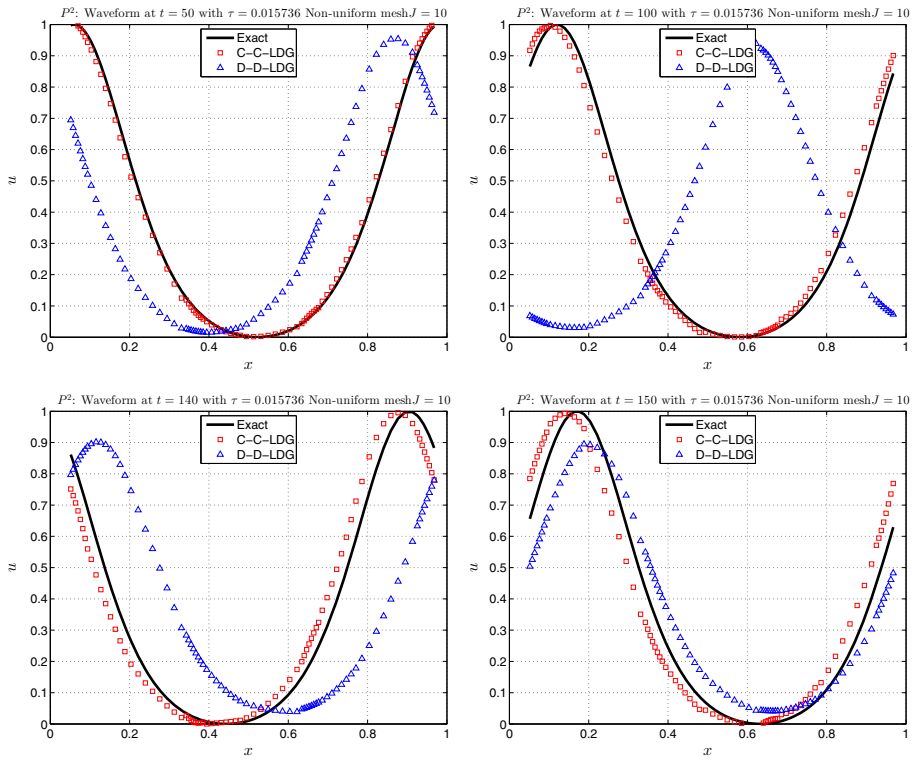

Fig. 9 Non-uniform meshes: the comparison of the waveform of C-C-LDG and D-D-LDG methods at different times $t = 50, 100, 140, 150$ in the cnoidal-wave example, with $\tau = 0.015736$, non-uniform spatial cells $J = 10$ and P^2 polynomial basis

The equations can be rewritten into a first order system by substituting u_x with variable v and g_x with variable w:

$$\begin{cases} u_t - \varepsilon v_{xt} + f(u)_x = 0, \\ v = u_x, \\ g_t - \varepsilon w_{xt} = 0, \\ w = g_x, \end{cases} \tag{4.2}$$

where $f(u) = u^2/2$. The semi-discrete dLDG methods for the system (4.2) are defined as follows: find u_h, v_h, g_h, and $w_h \in V_h^k$, such that for all test functions $\phi_1, \phi_2, \phi_3, \phi_4 \in V_h^k$ it holds that

$$\begin{cases} (u_{h,t}, \phi_1)_j + \varepsilon \mathcal{H}_j^*(v_{h,t}, \phi_1; \widehat{v_{h,t}}) - \mathcal{F}_j^*(u_h, \phi_1; \widehat{f}) = 0, \\ (v_h, \phi_2)_j + \mathcal{H}_j^*(u_h, \phi_2; \widehat{u_h}) = 0, \\ (g_{h,t}, \phi_3)_j + \varepsilon \mathcal{H}_j^*(w_{h,t}, \phi_3; \widehat{w_{h,t}}) = 0, \\ (w_h, \phi_4)_j + \mathcal{H}_j^*(g_h, \phi_4; \widehat{g_h}) = 0, \end{cases} \tag{4.3}$$

where the numerical flux of the nonlinear term $\widehat{f}$ can be chosen as the conservative flux (2.11) and the hatted numerical fluxes $\widehat{u_h}$, $\widehat{v_{h,t}}$, $\widehat{g_h}$ and $\widehat{w_{h,t}}$ are chosen as:

$$\begin{cases} \widehat{v_{h,t}} = \{v_{h,t}\} + k_1[w_{h,t}], \\ \widehat{u_h} = \{u_h\} + k_2[g_h], \\ \widehat{w_{h,t}} = \{w_{h,t}\} - k_2[v_{h,t}], \\ \widehat{g_h} = \{g_h\} - k_1[u_h], \end{cases} \tag{4.4}$$

and the parameters k_1, k_2 satisfies $k_1 k_2 = -1/4$. The average $\{\cdot\}$ in (4.4) can also be replaced by the generalized alternating numerical flux (2.10). Optimal error estimate cannot be obtained for the LDG method in Sect. 2 when average is used (i.e., Central-LDG method), and we will show that by this doubling-the-unknowns technique, one could recover the optimal error estimate.

4.1 Energy Conservation Property

In this subsection we present the energy conservation property of the dLDG scheme. The equations of u_h, v_h in the dLDG method (4.3) are the same as in the LDG method (2.2)–(2.2b), except the definition of the numerical fluxes are different. Therefore, Theorem 2.1 (mass conservation property) and Lemma 2.3 still hold, with the new definition of these fluxes. For the new variables g_h and w_h, we have the following lemma:

Lemma 4.1 *Let g_h, w_h be the solutions of dLDG scheme* (4.3), *the following result hold*

$$\frac{1}{2}\frac{d}{dt}\int_I \left(g_h^2 + \varepsilon w_h^2\right) dx + \varepsilon \sum_j \left((\widehat{w_{h,t}} - \{w_{h,t}\})[g_h] + (\widehat{g_h} - \{g_h\})[w_{h,t}]\right)_{j+\frac{1}{2}} = 0.$$

The proof of this Lemma follows that of Lemma 2.3, and is omitted here. Therefore, we have the following properties.

Theorem 4.1 *Let u_h, v_h, g_h and w_h be the solutions of dLDG scheme (4.3), with the numerical fluxes chosen as (4.4) and (2.11). The following energy conservation property holds*

$$dE_h(t) := \int_I \left(u_h^2(x,t) + \varepsilon v_h^2(x,t) + g_h^2(x,t) + \varepsilon w_h^2(x,t) \right) dx = dE_h(0). \quad (4.5)$$

Remark 4.1 Due to the introduction of auxiliary zero function g, the energy of dLDG method in (4.5) now include both u_h, v_h, and g_h, w_h, which is different from the conventional LDG method. This should be an approximate of the energy, because g_h and w_h are numerical approximation of zero functions, and we refer to [36] for more discussions on this matter.

4.2 Optimal Error Estimate

To derive the error estimate, the standard L^2 projections of the solutions v, w

$$\pi^v v = \pi v, \qquad \pi^w w = \pi w, \quad (4.6)$$

and the following coupled projections $\langle \pi^u, \pi^g \rangle$ of u and g

$$\begin{cases} (\pi^u u, \phi)_j = (u, \phi)_j, & \forall \phi \in P^{k-1}(I_j), \\ (\pi^g g, \phi)_j = (g, \phi)_j, & \forall \phi \in P^{k-1}(I_j), \\ \left(\{\pi^u u\} + k_2[\pi^g g] \right)_{j-\frac{1}{2}} = u(x_{j-\frac{1}{2}}), \\ \left(\{\pi^g g\} - k_1[\pi^u u] \right)_{j-\frac{1}{2}} = g(x_{j-\frac{1}{2}}), \end{cases} \quad (4.7)$$

are defined for all $j = 1, 2, \ldots, J$, where $k_1 k_2 = -1/4$ is assumed. At a first glance, the projections (4.7) seem to be globally coupled over all the element I_j, due to the appearance of $\{\cdot\}$ and $[\cdot]$ in the definition of the cell boundary terms. The following Lemma, following similar result in [36], shows that they are actually local projections with optimal projection errors.

Lemma 4.2 *The projections in (4.7) are well-defined, and they satisfy*

$$\begin{cases} \pi^u u = \dfrac{1}{2}\pi^+(u + 2k_2 g) + \dfrac{1}{2}\pi^-(u - 2k_2 g), \\ \pi^g g = \dfrac{1}{4k_2}\pi^+(u + 2k_2 g) - \dfrac{1}{4k_2}\pi^-(u - 2k_2 g). \end{cases} \quad (4.8)$$

In particular,

$$\|\pi^u u - u\|_0 \le Ch^{k+1} \quad and \quad \|\pi^g g - g\|_0 \le Ch^{k+1}. \quad (4.9)$$

Proof From the definition of the coupled projections (4.7), we know that for any α and β

$$(\alpha \pi^u u + \beta \pi^g g, \phi)_j = (\alpha u + \beta g, \phi)_j, \qquad \forall \phi \in P^{k-1}(I_j),$$

$$\left(\{\alpha \pi^u u + \beta \pi^g g\} + \frac{1}{2}[2\alpha k_2 \pi^g g - 2\beta k_1 \pi^u u] \right)\bigg|_{j-\frac{1}{2}} = \alpha u(x_{j-\frac{1}{2}}) + \beta g(x_{j-\frac{1}{2}}). \quad (4.10)$$

We can choose $\alpha = 1$, $\beta = 2k_2$ such that $2\alpha k_2 = \beta$, $-2\beta k_1 = \alpha$, since $k_1 k_2 = -1/4$. Note that for any $w \in V_h^k$ it holds $\{w\} + \frac{1}{2}[w] = w^+$, then the Eq. (4.10) leads to

$$\pi^u u + 2k_2 \pi^g g = \pi^+(u + 2k_2 g). \quad (4.11)$$

Similarly we can choose $\alpha = 1$, $\beta = -2k_2$ to derive

$$\pi^u u - 2k_2 \pi^g g = \pi^+(u - 2k_2 g). \tag{4.12}$$

The conclusion (4.8) follows from (4.11) and (4.12), and the error estimate (4.9) is the direct consequence of applying the error estimate (2.15) to $\pi^\pm$.   □

The following lemma is the analogue of Lemma 2.4.

Lemma 4.3 *Suppose (u_h, v_h), $(g_h, w_h) \in V_h^k \times V_h^k$ are the solutions of the dLDG methods (4.3) with the numerical fluxes (4.4), and the projections (4.6) and (4.7) are used, then there exists a positive constant C, which is independent of h, such that*

$$\|\xi_{u,x}\|_0 + h^{-1/2}|[\xi_u]| \leq C \left(\|\xi_v\|_0 + \|\xi_w\|_0 \right), \tag{4.13}$$

$$\|\xi_{g,x}\|_0 + h^{-1/2}|[\xi_g]| \leq C \left(\|\xi_v\|_0 + \|\xi_w\|_0 \right). \tag{4.14}$$

Proof From the second and fourth equations of (4.3), we can obtain

$$(v_h + 2k_2 w_h, \phi)_j + \mathcal{H}_j^*(u_h + 2k_2 g_h, \phi; \widehat{u_h} + 2k_2 \widehat{g_h}) = 0,$$

$$(v_h - 2k_2 w_h, \phi)_j + \mathcal{H}_j^*(u_h - 2k_2 g_h, \phi; \widehat{u_h} - 2k_2 \widehat{g_h}) = 0,$$

with the fluxes satisfying

$$\widehat{u_h} + 2k_2 \widehat{g_h} = (u_h + 2k_2 g_h)^+, \qquad \widehat{u_h} - 2k_2 \widehat{g_h} = (u_h - 2k_2 g_h)^-.$$

Therefore, $\langle u_h + 2k_2 g_h, v_h + 2k_2 w_h \rangle$ and $\langle u_h - 2k_2 g_h, v_h - 2k_2 w_h \rangle$ satisfy the assumptions of Lemma 2.4, and we have

$$\|\xi_{u,x} + 2k_2 \xi_{g,x}\|_0 + h^{-1/2}|[\xi_u + 2k_2 \xi_g]| \leq C\|\xi_v + 2k_2 \xi_w\|_0 \leq C \left(\|\xi_v\|_0 + \|\xi_w\|_0 \right), \tag{4.15}$$

$$\|\xi_{u,x} - 2k_2 \xi_{g,x}\|_0 + h^{-1/2}|[\xi_u - 2k_2 \xi_g]| \leq C\|\xi_v - 2k_2 \xi_w\|_0 \leq C \left(\|\xi_v\|_0 + \|\xi_w\|_0 \right), \tag{4.16}$$

and the results (4.13) and (4.14) follow from the fact that $\xi_u = \frac{1}{2}(\xi_u + 2k_2 \xi_g) + \frac{1}{2}(\xi_u - 2k_2 \xi_g)$ and $\xi_g = \frac{1}{4k_2}(\xi_u + 2k_2 \xi_g) - \frac{1}{4k_2}(\xi_u - 2k_2 \xi_g)$.   □

Theorem 4.2 *Let u_h, v_h, g_h and w_h be the numerical solutions of dLDG scheme (4.3) with the numerical fluxes (4.4), and the numerical flux of the nonlinear term $\widehat{f}(u^-, u^+)$ chosen as (2.11). Let u, v, g and w be the exact solution of the problem (4.2) which are sufficiently smooth. For small h and all $t \in [0, T]$, it holds that*

$$\|e_u\| \leq Ch^{k+1}, \quad \|e_v\| \leq Ch^{k+1}, \quad \|e_g\| \leq Ch^{k+1}, \quad \|e_w\| \leq Ch^{k+1}. \tag{4.17}$$

where the constant C may depend on T, k, the length of the domain I and some Sobolev norms of the exact solutions up to time T, but is independent of h.

The proof follows the same line as that of Theorem 2.4, and is skipped to save space.

4.3 Temporal Discretization

The fully discrete dLDG methods, coupled with the implicit midpoint temporal discretization, will be discussed in this section. They take the following form: we are looking for the solutions u_h^{n+1}, v_h^{n+1}, g_h^{n+1} and w_h^{n+1} for $n = 1, 2, \ldots, N - 1$, such that

$$\begin{cases} (\delta_t^+ u_h^n, \phi_1)_j + \varepsilon \mathcal{H}_j^*(\delta_t^+ v_h^n, \phi_1; \widehat{\delta_t^+ v_h^n}) - \mathcal{F}_j^*(u_h^{n+\frac{1}{2}}, \phi_1; \widehat{f}^{n+\frac{1}{2}}) = 0, \\ (v_h^{n+\frac{1}{2}}, \phi_2)_j + \mathcal{H}_j^*(u_h^{n+\frac{1}{2}}, \phi_2; (\widehat{u_h})^{n+\frac{1}{2}}) = 0, \\ (\delta_t^+ g_h^n, \phi_3)_j + \varepsilon \mathcal{H}_j^*(\delta_t^+ w_h^n, \phi_3; \widehat{\delta_t^+ w_h^n}) = 0, \\ (w_h^{n+\frac{1}{2}}, \phi_4)_j + \mathcal{H}_j^*(g_h^{n+\frac{1}{2}}, \phi_4; (\widehat{g_h})^{n+\frac{1}{2}}) = 0, \end{cases} \qquad (4.18)$$

hold for all test functions ϕ_1, ϕ_2, ϕ_3 and $\phi_4 \in V^k$ on every cell I_j. Here the nonlinear numerical flux $\widehat{f}^{n+\frac{1}{2}}$ can be chosen as (2.11), and the other numerical fluxes $\widehat{\delta_t^+ v_h^n}$, $(\widehat{u_h})^{n+\frac{1}{2}}$, $\widehat{\delta_t^+ w_h^n}$, $\widehat{(g_h)}^{n+\frac{1}{2}}$ take the similar form as (4.4)

$$\begin{cases} \widehat{\delta_t^+ v_h^n} = \{\delta_t^+ v_h^n\} + k_1[\delta_t^+ w_h^n], \\ (\widehat{u_h})^{n+\frac{1}{2}} = \{u_h^{n+\frac{1}{2}}\} + k_2[g_h^{n+\frac{1}{2}}], \\ \widehat{\delta_t^+ w_h^n} = \{\delta_t^+ w_h^n\} - k_2[\delta_t^+ v_h^n], \\ \widehat{(g_h)}^{n+\frac{1}{2}} = \{g_h^{n+\frac{1}{2}}\} - k_1[u_h^{n+\frac{1}{2}}], \end{cases} \qquad (4.19)$$

where $k_1 k_2 = -1/4$.

The mass and energy conservation property of the fully discrete dLDG methods is summarized below.

Theorem 4.3 *Let* u_h^n, v_h^n, g_h^n *and* w_h^n *be the solutions of the fully discrete dLDG methods* (4.18). *With the discrete mass and energy defined as*

$$M_h^n = \int_I u_h^n dx, \qquad E_h^n = \int_I \left((u_h^n)^2 + \varepsilon(v_h^n)^2 + (g_h^n)^2 + \varepsilon(w_h^n)^2\right) dx, \qquad (4.20)$$

the following mass conservation and energy dissipative property holds for any n

$$M_h^n = M_h^0, \qquad E_h^n = E_h^0. \qquad (4.21)$$

The implementation of the fully discrete dLDG methods (4.18) is similar to that of the LDG methods as discussed at the end of Sect. 2.4. The two additional equations are both linear. As the implicit temporal discretization is used, most of the computational time is spent on the nonlinear equation, therefore the computational cost of the dLDG method is not significantly more than that of the LDG method, which will be discussed in the numerical example section.

5 Numerical Experiments of the dLDG Methods

In this section, we provide some numerical results of the proposed dLDG methods with implicit midpoint temporal discretization. The accuracy test and the comparison of the dLDG and LDG methods will be studied. $k_1 = 1/2$ and $k_2 = -1/2$ are chosen in the numerical experiments.

5.1 Accuracy Test

The same cnoidal-wave solution (1.4), studied in Sect. 3.1, is considered here to verify the convergence rate. The numerical error are computed at the stopping time $T = 1$. Similarly, we set the time-step as $\tau = 0.5877h^2$. Numerical order of accuracy of the dLDG method is given in Tables 10 and 11. Optimal order of accuracy of u_h, g_h, v_h, w_h can be observed with P^k, $k = 1, 2, 3$, basis functions, when the coupled projections $\langle \pi^u, \pi^g \rangle$ are chosen to evaluate the numerical initial conditions. When L^2 projection is used, optimal order of accuracy of u_h and g_h still can be observed, while the accuracy of v_h and w_h are not optimal any more (see Table 11). Note that the Central-LDG method delivers suboptimal error estimate of u_h, and by doubling the unknowns, the proposed dLDG method gives optimal convergence rate. We have also tested other choices of k_1, k_2 (satisfying $k_1 k_2 = -1/4$), and observe the same behavior.

Figure 10 shows the time history of the error of mass and energy (i.e., $M_h^N - M_h^0$ and $E_h^N - E_h^0$) of the dLDG methods, where we can see that the mass and energy are both exactly preserved to the machine error at the level of 10^{-14}.

5.2 Comparison of the dLDG and LDG Methods

Both the dLDG and C-C-LDG methods are optimal energy conserving methods for the BBM equation. A numerical comparison of these two methods is conducted in this section.

To provide a fair comparison, we provide the numerical results of the dLDG method with J elements, as well as the C-C-LDG methods with both J and $2J$ elements. In Fig. 11, we plot the time history of the L^2 errors of u_h of C-C-LDG ($J = 10$ and $J = 20$) and dLDG ($J = 10$) methods with various P^k basis, for the same cnoidal-wave example. The stopping time is set as $T = 10$ with $N = 5120$ uniform time steps. We can see the L^2 error of the dLDG ($J = 10$) methods is between those of the C-C-LDG ($J = 10$) and C-C-LDG ($J = 20$) methods, for all of P^1, P^2 and P^3 spaces. For P^2 and P^3 case, the growth rate of L^2 error of the dLDG ($J = 10$) method is similar to that of the C-C-LDG ($J = 20$), while the initial error of the dLDG method at $t = 0$ is larger since less elements are used. It's worth noting that for P^0 case the L^2 error of dLDG ($J = 10$) and C-C-LDG ($J = 10$) methods are the same, because one can actually show that with P^0 basis the dLDG scheme simply reduces to the C-C-LDG scheme.

In Table 12, we list the average computational times (by taking the average of 20 runs) of C-C-LDG and dLDG methods with different J and various P^k basis. It can be observed that, with the same number of elements and P^k basis, the computational times of C-C-LDG and dLDG method are almost the same, since most of the computation is spent on solving the nonlinear equation when the implicit temporal discretization is used. In general, our computational tests suggest that, with the same number of elements, the dLDG method provides a smaller error than the LDG method, while maintaining slightly larger computational cost.

6 Conclusion Remarks

In this paper, we develop, analyze and numerically validate two classes of LDG methods for solving the nonlinear BBM equation. By introducing one auxiliary variable, and with appropriately chosen numerical fluxes, the conventional LDG methods can be shown to preserve the discrete version of mass, and either preserve or dissipate the discrete version of

Table 10 Numerical error and convergence orders of u, v, g and w of **dLDG** scheme in the cnoidal-wave example

h	τ	Error of u				Error of g			
		$\|e_u\|_2$	C_2	$\|e_u\|_\infty$	C_∞	$\|e_g\|_2$	C_2	$\|e_g\|_\infty$	C_∞
P^0									
h_1	τ_1	9.7160E−02	*	3.0943E−01	*	2.2534E−16	*	5.2780E−16	*
$h_1/2$	$\tau_1/4$	3.8744E−02	1.3264	1.3342E−01	1.2136	4.4211E−16	−0.9723	1.0015E−15	−0.9241
$h_1/4$	$\tau_1/16$	1.7500E−02	1.1467	5.8275E−02	1.1951	2.6712E−15	−2.5950	8.6103E−15	−3.1039
$h_1/8$	$\tau_1/64$	8.4438E−03	1.0446	2.6686E−02	1.1268	1.5930E−14	−2.5762	5.7527E−14	−2.7401
P^1									
h_1	τ_1	1.0041E−02	*	4.2002E−02	*	9.8597E−03	*	4.0930E−02	*
$h_1/2$	$\tau_1/4$	2.0548E−03	2.2888	1.0773E−02	1.9630	2.4344E−03	2.0180	1.0709E−02	1.9344
$h_1/4$	$\tau_1/16$	4.7856E−04	2.1022	2.5421E−03	2.0833	6.0452E−04	2.0097	2.6314E−03	2.0249
$h_1/8$	$\tau_1/64$	1.1747E−04	2.0265	6.1524E−04	2.0468	1.5083E−04	2.0029	6.6012E−04	1.9951
P^2									
h_1	τ_1	7.5839E−04	*	2.5865E−03	*	7.8016E−04	*	3.5158E−03	*
$h_1/2$	$\tau_1/4$	9.2759E−05	3.0314	3.8322E−04	2.7548	1.0611E−04	2.8782	4.6019E−04	2.9336
$h_1/4$	$\tau_1/16$	1.1604E−05	2.9989	5.0728E−05	2.9173	1.3620E−05	2.9618	6.0548E−05	2.9261
$h_1/8$	$\tau_1/64$	1.4511E−06	2.9993	6.3764E−06	2.9920	1.7136E−06	2.9906	7.5849E−06	2.9969
P^3									
h_1	τ_1	7.1272E−05	*	3.2366E−04	*	8.0328E−05	*	4.2503E−04	*
$h_1/2$	$\tau_1/4$	4.5332E−06	3.9748	2.2786E−05	3.8283	5.0663E−06	3.9869	2.9548E−05	3.8464
$h_1/4$	$\tau_1/16$	2.8385E−07	3.9973	1.3737E−06	4.0520	3.1549E−07	4.0053	1.7889E−06	4.0460
$h_1/8$	$\tau_1/64$	1.7747E−08	3.9995	8.7278E−08	3.9763	1.9692E−08	4.0019	1.1283E−07	3.9868

Table 10 continued

h	τ	Error of v				Error of w			
		$\|e_v\|_2$	C_2	$\|e_v\|_\infty$	C_∞	$\|e_w\|_2$	C_2	$\|e_w\|_\infty$	C_∞
P^0									
h_1	τ_1	9.6742E−01	*	3.0883E+00	*	8.6046E−01	*	1.8311E+00	*
$h_1/2$	$\tau_1/4$	3.8888E−01	1.3148	1.7602E+00	0.8111	5.0862E−01	0.7585	1.2838E+00	0.5123
$h_1/4$	$\tau_1/16$	1.6828E−01	1.2085	8.0961E−01	1.1204	2.6711E−01	0.9292	6.9921E−01	0.8766
$h_1/8$	$\tau_1/64$	7.9944E−02	1.0738	3.7430E−01	1.1131	1.3527E−01	0.9816	3.5781E−01	0.9665
P^1									
h_1	τ_1	1.4126E−01	*	6.5876E−01	*	3.3699E−01	*	1.0276E+00	*
$h_1/2$	$\tau_1/4$	2.8772E−02	2.2957	1.3716E−01	2.2639	9.7827E−02	1.7844	3.1732E−01	1.6953
$h_1/4$	$\tau_1/16$	6.3271E−03	2.1850	3.0134E−02	2.1864	2.5497E−02	1.9399	8.4203E−02	1.9140
$h_1/8$	$\tau_1/64$	1.5137E−03	2.0635	7.0816E−03	2.0893	6.4429E−03	1.9845	2.1310E−02	1.9823
P^2									
h_1	τ_1	2.1206E−02	*	8.5122E−02	*	1.0468E−02	*	3.3861E−02	*
$h_1/2$	$\tau_1/4$	1.9059E−03	3.4759	9.1750E−03	3.2138	2.0033E−03	2.3855	8.4697E−03	1.9992
$h_1/4$	$\tau_1/16$	2.0553E−04	3.2131	1.1623E−03	2.9807	2.8634E−04	2.8066	1.2134E−03	2.8033
$h_1/8$	$\tau_1/64$	2.4375E−05	3.0759	1.4061E−04	3.0472	3.7069E−05	2.9494	1.5818E−04	2.9394
P^3									
h_1	τ_1	1.6667E−03	*	9.0108E−03	*	2.1228E−03	*	9.1223E−03	*
$h_1/2$	$\tau_1/4$	9.4049E−05	4.1474	4.9856E−04	4.1758	1.3160E−04	4.0117	6.3136E−04	3.8528
$h_1/4$	$\tau_1/16$	5.6605E−06	4.0544	2.8437E−05	4.1319	8.3131E−06	3.9846	4.1576E−05	3.9247
$h_1/8$	$\tau_1/64$	3.4923E−07	4.0187	1.6788E−06	4.0823	5.2127E−07	3.9953	2.6013E−06	3.9984

Coupled Projection $\langle\{\pi^u\}, \{\pi^8\}\rangle$ for u_0 and g_0 with $k_1 = \frac{1}{2}$, $k_2 = -\frac{1}{2}$, $x_l = 0$, $x_r = 0.92237$, $T = 1$, $h_1 = 9.2237E\text{-}02$, $\tau_1 = 0.005$

Table 11 Numerical error and convergence orders of u, v, g and w of **dLDG** scheme in the cnoidal-wave example

h	τ	Error of u				Error of g			
		$\|e_u\|_2$	C_2	$\|e_u\|_\infty$	C_∞	$\|e_g\|_2$	C_2	$\|e_g\|_\infty$	C_∞
P^0									
h_1	τ_1	9.7160E−02	*	3.0943E−01	*	2.2534E−16	*	5.2780E−16	*
$h_1/2$	$\tau_1/4$	3.8744E−02	1.3264	1.3342E−01	1.2136	4.4211E−16	-0.9723	1.0015E−15	−0.9241
$h_1/4$	$\tau_1/16$	1.7500E−02	1.1467	5.8275E−02	1.1951	2.6712E−15	−2.5950	8.6103E−15	−3.1039
$h_1/8$	$\tau_1/64$	8.4838E−03	1.0446	2.6686E−02	1.1268	1.5930E−14	−2.5762	5.7527E−14	−2.7401
P^1									
h_1	τ_1	1.0202E−02	*	4.1618E−02	*	1.5934E−02	*	4.9514E−02	*
$h_1/2$	$\tau_1/4$	2.0757E−03	2.2972	1.0701E−02	1.9594	4.0100E−03	1.9905	1.3165E−02	1.9111
$h_1/4$	$\tau_1/16$	4.8003E−04	2.1124	2.5326E−03	2.0791	9.9999E−04	2.0036	3.2907E−03	2.0003
$h_1/8$	$\tau_1/64$	1.1756E−04	2.0297	6.1406E−04	2.0441	2.4974E−04	2.0015	8.2026E−04	2.0042
P^2									
h_1	τ_1	7.6014E−04	*	2.4753E−03	*	1.1722E−03	*	3.5156E−03	*
$h_1/2$	$\tau_1/4$	9.2563E−05	3.0378	3.8163E−04	2.6974	1.5995E−04	2.8735	5.0965E−04	2.7862
$h_1/4$	$\tau_1/16$	1.1594E−05	2.9970	5.0398E−05	2.9207	2.0547E−05	2.9606	6.5073E−05	2.9694
$h_1/8$	$\tau_1/64$	1.4508E−06	2.9985	6.3720E−06	2.9835	2.5865E−06	2.9898	8.1996E−06	2.9884
P^3									
h_1	τ_1	7.0885E−05	*	3.2373E−04	*	1.0447E−04	*	4.1177E−04	*
$h_1/2$	$\tau_1/4$	4.5324E−06	3.9671	2.2724E−05	3.8325	6.7235E−06	3.9578	2.9102E−05	3.8226
$h_1/4$	$\tau_1/16$	2.8386E−07	3.9970	1.3707E−06	4.0512	4.1855E−07	4.0057	1.7835E−06	4.0284
$h_1/8$	$\tau_1/64$	1.7748E−08	3.9995	8.7195E−08	3.9745	2.6121E−08	4.0021	1.1166E−07	3.9975

Table 11 continued

h	τ	Error of v				Error of w			
		$\|e_v\|_2$	C_2	$\|e_v\|_\infty$	C_∞	$\|e_w\|_2$	C_2	$\|e_w\|_\infty$	C_∞
P^0									
h_1	τ_1	9.6742E−01	*	3.0883E+00	*	8.6046E−01	*	1.8311E+00	*
$h_1/2$	$\tau_1/4$	3.8888E−01	1.3148	1.7602E+00	0.8111	5.0862E−01	0.7585	1.2838E+00	0.5123
$h_1/4$	$\tau_1/16$	1.6828E−01	1.2085	8.0961E−01	1.1204	2.6711E−01	0.9292	6.9921E−01	0.8766
$h_1/8$	$\tau_1/64$	7.9944E−02	1.0738	3.7430E−01	1.1131	1.3527E−01	0.9816	3.5781E−01	0.9665
P^1									
h_1	τ_1	5.9063E−01	*	2.1175E+00	*	3.6518E−01	*	1.3737E+00	*
$h_1/2$	$\tau_1/4$	3.0932E−01	0.9331	1.2814E+00	0.7246	1.0313E−01	1.8242	3.7504E−01	1.8729
$h_1/4$	$\tau_1/16$	1.5631E−01	0.9847	6.7425E−01	0.9264	2.6761E−02	1.9462	9.7062E−02	1.9501
$h_1/8$	$\tau_1/64$	7.8365E−02	0.9961	3.4140E−01	0.9818	6.7581E−03	1.9855	2.4406E−02	1.9917
P^2									
h_1	τ_1	5.0810E−02	*	2.6674E−01	*	6.3399E−02	*	2.8750E−01	*
$h_1/2$	$\tau_1/4$	6.2826E−03	3.0157	3.2869E−02	3.0206	1.7876E−02	1.8264	7.2100E−02	1.9955
$h_1/4$	$\tau_1/16$	7.7837E−04	3.0128	3.8679E−03	3.0871	4.5817E−03	1.9641	1.7875E−02	2.0120
$h_1/8$	$\tau_1/64$	9.6984E−05	3.0046	4.7035E−04	3.0398	1.1517E−03	1.9921	4.4402E−03	2.0093
P^3									
h_1	τ_1	9.5170E−03	*	5.9544E−02	*	8.2275E−03	*	4.8253E−02	*
$h_1/2$	$\tau_1/4$	1.6232E−03	2.5516	1.1457E−02	2.3777	6.9832E−04	3.5585	4.5610E−03	3.4032
$h_1/4$	$\tau_1/16$	2.2163E−04	2.8726	1.6305E−03	2.8129	4.6942E−05	3.8950	3.1249E−04	3.8674
$h_1/8$	$\tau_1/64$	2.8347E−05	2.9669	2.1098E−04	2.9501	2.9900E−06	3.9726	2.0411E−05	3.9364

L^2 **Projection** π for u_0 and g_0 with $k_1 = \frac{1}{2}$, $k_2 = -\frac{1}{2}$, $x_l = 0$, $x_r = 0.92237$, $T = 1$, $h_1 = 9.2237E\text{-}02$, $\tau_1 = 0.005$
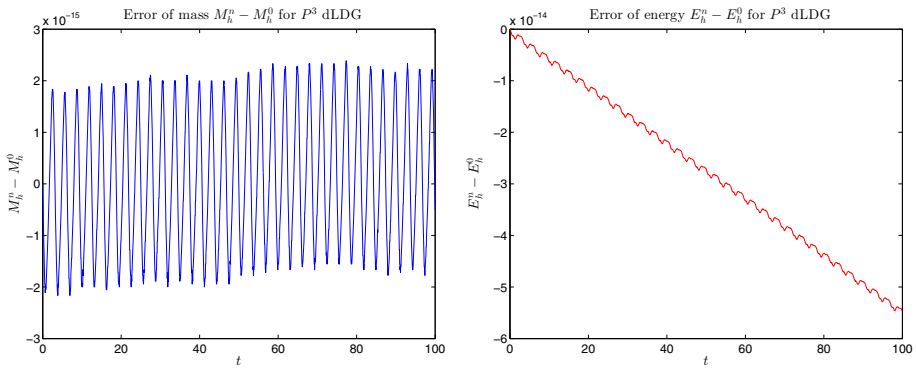
Fig. 10 Errors of mass (left) and energy (right) of the dLDG method in Sect. 5.1 with $J = 10, T = 100$, $N = 2480$ and P^3 polynomial basis
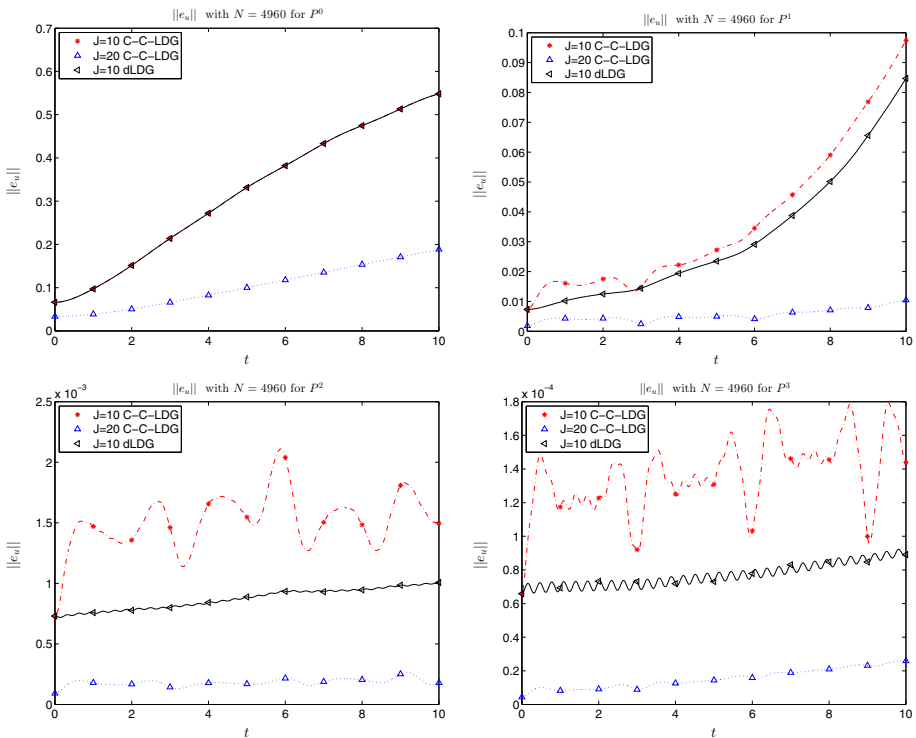

Fig. 11 Time history of the numerical errors of u_h in L^2 norm with uniform time cells $N = 4960$ for $T = 10$ of C-C-LDG ($J = 10$ and $J = 20$) and dLDG ($J = 10$) methods in the cnoidal-wave example with P^0 (top left), P^1 (top right), P^2 (bottom left) and P^3 (bottom right) polynomial basis

Table 12 Average computational times (in seconds) of 20 runs of C-C-LDG and dLDG method with $N = 5120$, $T = 10$, $x_l = 0$, $x_r = 0.92237$ and different J in the cnoidal-wave example

	$J = 50$		$J = 100$		$J = 200$	
	C-C-LDG	dLDG	C-C-LDG	dLDG	C-C-LDG	dLDG
P^0	3.6000	3.7227	4.2211	4.3125	6.4695	6.6383
P^1	3.2781	3.3820	4.3273	4.5594	17.5703	17.7000
P^2	3.5500	3.8281	5.3578	5.8336	29.4523	31.6195
P^3	3.9766	4.3367	6.5313	7.2875	42.3992	46.5656

energy of the continuous solution, up to the round-off level. One contribution of the paper is to provide an optimal a priori error estimate for both the semi-discrete energy conserving and energy dissipative methods applied to the nonlinear BBM equation. To achieve this goal, we discover the connection between the error of the auxiliary and primary variables, and use it to bound the nonlinear term by the auxiliary variable. Fully discrete methods can be derived by coupled with energy-conserving implicit midpoint temporal discretization. Numerical experiments confirm the optimal rates of convergence, and the advantage of energy conserving method for long time simulation. We also present another class of energy conserving LDG methods for the nonlinear BBM equation, based on the doubling-the-unknowns technique in [36]. We investigate their energy conservation property, optimal convergence rate, and numerical comparison of these two energy conserving LDG methods.

References

1. Bona, J.L., Smith, R.: The initial-value problem for the Korteweg–de Vries equation. Philos. Trans. R. Soc. Lond. Ser. B Biol. Sci. **278**, 555–601 (1975)
2. Benjamin, T., Bona, J., Mahony, J.: Model equations for long waves in nonlinear dispersive systems. Philos. Trans. R. Soc. Lond. Ser. A Math. Phys. Sci. **272**, 47–78 (1972)
3. Abbasbandy, S., Shirzadi, A.: The first integral method for modified Benjamin–Bona–Mahony equation. Commun. Nonlinear Sci. Numer. Simul. **15**, 1759–1764 (2010)
4. Wazwaz, A.M.: Exact solution with compact and non-compact structures for the one-dimensional generalized Benjamin–Bona–Mahony equation. Commun. Nonlinear Sci. Numer. Simul. **10**, 855–867 (2005)
5. Omrani, K.: The convergence of fully discrete Galerkin approximations for the Benjamin–Bona–Mahony (BBM) equation. Appl. Math. Comput. **180**, 614–621 (2006)
6. Abramowitz, M., Stegun, I.: editors, Handbook of Mathematical Functions with Formulas, Graphs, and Mathematical Tables, volume 55 of Applied Mathematics Series, National Bureau of Standards, MR167642 (1965)
7. Avrin, J., Goldstein, J.A.: Global existence for the Benjamin–Bona–Mahony equation in arbitrary dimensions. Nonlinear Anal. **9**, 861–865 (1985)
8. Goldstein, J.A., Wichnoski, B.: On the Benjamin–Bona–Mahony equation in higher dimensions. Nonlinear Anal. **4**, 665–675 (1980)
9. Medeiros, L.A., Menzela, G.P.: Existence and uniqueness for periodic solutions of the Benjamin–Bona–Mahony equation. SIAM J. Math. Anal. **8**, 792–799 (1977)
10. Wang, L., Zhou, J., Ren, L.: The exact solitary wave solutions for a family of BBM equation. Int. J. Nonlinear Sci. **1**, 58–64 (2006)
11. Achouri, T., Khiari, N., Omrani, K.: On the convergence of difference schemes for the Benjamin–Bona–Mahony (BBM) equation. Appl. Math. Comput. **182**, 999–1005 (2006)
12. Omrani, K., Ayadi, M.: Finite difference discretization of the Benjamin–Bona–Mahony–Burgers (BBMB) equation. Numer. Methods Partial Differ. Equ. **24**, 239–248 (2008)
13. Gao, F., Qiu, J., Zhang, Q.: Local discontinuous Galerkin finite element method and error estimates for one class of Sobolev equation. J. Sci. Comput. **41**, 436–460 (2009)

14. Zhang, Q., Gao, F.: A fully-discrete local discontinuous Galerkin method for convection-dominated Sobolev equation. J. Sci. Comput. **51**, 107–134 (2012)
15. Kamga, A., Mitsotakis, D.: A high order discontinuous Galerkin method for the convection dominated KdV–BBM equation and its efficient implementation, preprint available on researchgate.net
16. Buli, J., Xing, Y.: Local discontinuous Galerkin methods for the Boussinesq coupled BBM system. J. Sci. Comput. **75**, 536–559 (2018)
17. Cockburn, B., Hou, S., Shu, C.-W.: The Runge–Kutta local projection discontinuous Galerkin finite element method for conservation laws IV: the multidimensional case. Math. Comput. **54**, 545–581 (1990)
18. Cockburn, B., Karniadakis, G., Shu, C.-W.: The development of discontinuous Galerkin methods, In: Cockburn, B., Karniadakis, G., Shu, C.-W. (eds.) Discontinuous Galerkin Methods: Theory, Computation and Applications, pp. 3–50. Lecture Notes in Computational Science and Engineering, Part I: Overview, Vol. 11, Springer, Berlin (2000)
19. Cockburn, B., Lin, S.-Y., Shu, C.-W.: TVB Runge–Kutta local projection discontinuous Galerkin finite element method for conservation laws III: one dimensional systems. J. Comput. Phys. **84**, 90–113 (1989)
20. Cockburn, B., Shu, C.-W.: TVB Runge–Kutta local projection discontinuous Galerkin finite element method for conservation laws II: general framework. Math. Comput. **52**, 411–435 (1989)
21. Reed, W.H., Hill, T.R.: Triangular mesh methods for the neutron transport equation, Technical Report LA-UR-73-479, Los Alamos Scientific Laboratory (1973)
22. Cockburn, B., Shu, C.W.: The local discontinuous Galerkin finite element method for convection-diffusion systems. SIAM J. Numer. Anal. **35**, 2440–2463 (1998)
23. Xu, Y., Shu, C.-W.: Local discontinuous Galerkin methods for high-order time-dependent partial differential equations. Commun. Comput. Phys. **7**, 1–46 (2010)
24. Bona, J.L., Chen, H., Karakashian, O.A., Xing, Y.: Conservative discontinuous Galerkin methods for the generalized Korteweg–de Vries equation. Math. Comput. **82**, 1401–1432 (2013)
25. Yi, N., Huang, Y., Liu, H.: A direct discontinuous Galerkin method for the generalized Korteweg–de Vries equation: energy conservation and boundary effect. J. Comput. Phys. **242**, 351–366 (2013)
26. Karakashian, O., Xing, Y.: A posteriori error estimates for conservative local discontinuous Galerkin methods for the generalized Korteweg–de Vries equation. Commun. Comput. Phys. **20**, 250–278 (2016)
27. Zhang, Q., Xia, Y.: Conservative and dissipative local discontinuous Galerkin methods for Korteweg–de Vries type equations. Commun. Comput. Phys. **25**, 532–563 (2019)
28. Xing, Y., Chou, C.-S., Shu, C.-W.: Energy conserving local discontinuous Galerkin methods for wave propagation problems. Inverse Probl. Imaging **7**, 967–986 (2013)
29. Chou, C.-S., Shu, C.-W., Xing, Y.: Optimal energy conserving local discontinuous Galerkin methods for second-order wave equation in heterogeneous media. J. Comput. Phys. **272**, 88–107 (2014)
30. Cheng, Y., Chou, C.-S., Li, F., Xing, Y.: L2 stable discontinuous Galerkin methods for one-dimensional two-way wave equations. Math. Comput. **86**, 121–155 (2017)
31. Liu, H., Xing, Y.: An invariant preserving discontinuous Galerkin method for the Camassa–Holm equation. SIAM J. Sci. Comput. **38**, A1919–A1934 (2016)
32. Huang, Y., Liu, H., Yi, N.: A conservative discontinuous Galerkin method for the Degasperis-Procesi equation. Methods Appl. Anal. **21**, 67–90 (2014)
33. Guo, L., Xu, Y.: Energy conserving local discontinuous Galerkin methods for the nonlinear Schrödinger equation with wave operator. J. Sci. Comput. **65**, 622–647 (2015)
34. Liang, X., Khaliq, A.Q.M., Xing, Y.: Fourth order exponential time differencing method with local discontinuous Galerkin approximation for coupled nonlinear Schrödinger equations. Commun. Comput. Phys. **17**, 510–541 (2015)
35. Li, X., Sun, W., Xing, Y., Chou, C.-S.: Energy conserving local discontinuous Galerkin methods for the improved Boussinesq equation. J. Comput. Phys. **401**, 109002 (2020)
36. Fu, G., Shu, C.-W.: Optimal energy-conserving discontinuous Galerkin methods for linear symmetric hyperbolic systems. J. Comput. Phys. **394**, 329–363 (2019)
37. Fu, G., Shu, C.-W.: An energy-conserving ultra-weak discontinuous Galerkin method for the generalized Korteweg–de Vries equation. J. Comput. Appl. Math. **349**, 41–51 (2019)
38. Meng, X., Shu, C.-W., Wu, B.: Optimal error estimates for discontinuous Galerkin methods based on upwind-biased fluxes for linear hyperbolic equations. Math. Comput. **85**, 1225–1261 (2016)
39. Cheng, Y., Meng, X., Zhang, Q.: Application of generalized Gauss–Radau projections for the local discontinuous Galerkin method for linear convection-diffusion equations. Math. Comput. **86**, 1233–1267 (2017)
40. Xu, Y., Shu, C.-W.: Error estimates of the semi-discrete local discontinuous Galerkin method for nonlinear convection diffusion and KdV equations. Comput. Methods Appl. Mech. Eng. **196**, 3805–3822 (2007)

41. Wang, H., Shu, C.-W., Zhang, Q.: Stability and error estimates of local discontinuous Galerkin method with implicit-explicit time-marching for advection-diffusion problems. SIAM J. Numer. Anal. **53**, 206–227 (2015)
42. Li, X.H., Shu, C.-W., Yang, Y.: Local discontinuous Galerkin method for the Keller–Segel chemotaxis model. J. Sci. Comput. **73**, 943–967 (2017)

Affiliations

Xiaole Li[1,2] · Yulong Xing[2] · **Ching-Shan Chou[2]**

✉ Yulong Xing
  xing.205@osu.edu

  Xiaole Li
  leeggwp@163.com

  Ching-Shan Chou
  chou@math.ohio-state.edu

1   College of Automation, Harbin Engineering University, Harbin 150001, China

2   Department of Mathematics, The Ohio State University, Columbus, OH 43210, USA